

**Bank of Israel**



**Research Department**

## **Global Warming Effects on Electricity Demand in Israel<sup>1</sup>**

**Tanya Suhoy\* and Maayan Tropper-Wachtel\*\***

Discussion Paper 2021.17

August 2021

---

Bank of Israel - <http://www.boi.org.il>

<sup>1</sup> We thank Nir Stav, the Director of the Israeli Meteorological Service (IMS), and Avner Furshpan, Yoav Levi, Yizhak Yosef, Eyal Amitai, Anat Baharad, Leenes Uzan and Vladimir Meerson from the IMS Climatology, Research, and IT departments for fruitful discussion, data, technological assistance, and advice on this study; Yehuda Porath and Eyal Argov from the Research Department of the Bank of Israel for discussion and help.

\* Tanya Suhoy - Research Department, Bank of Israel - Email: [tanya.suhoy@boi.org.il](mailto:tanya.suhoy@boi.org.il)

\*\* Maayan Tropper-Wachtel - Research Department, Bank of Israel - Email [maayantropp@gmail.com](mailto:maayantropp@gmail.com)

**Any views expressed in the Discussion Paper Series are those of the authors  
and do not necessarily reflect those of the Bank of Israel**

חטיבת המחקר, בנק ישראל ת"ד 780 ירושלים 91007

**Research Department, Bank of Israel. POB 780, 91007 Jerusalem, Israel**

# Global Warming Effects on Electricity Demand in Israel

Tanya Suhoy and Maayan Tropper-Wachtel

## Abstract

In this paper, we attempt to quantify the impact of climate change on future electricity demand in Israel, based on CORDEX-AFRICA high-resolution climate simulations made under two Representative Concentration Pathway scenarios (hereinafter: RCP 4.5 and 8.5), and further downscaled by the Israeli Meteorological Service (hereinafter: IMS) with regard to location of Israeli meteorological stations. We provide first estimates of this impact by comparing load forecasts based on RCP 4.5 and 8.5 with their counterparts based on historically observed temperatures, properly bootstrapped under an assumption of no warming trend.

We employ two methodological approaches: the first is based on dose-response functions and allows us to estimate the relationship between daily peak loads and daily maximum temperatures in a form comparable across countries. This provides evidence of a higher sensitivity of Israeli peak loads to rising temperatures compared to hot areas in other developed countries, such as Texas or the Australian states. The second approach employs an hourly-load econometric model for Israel.

With the present sensitivity level, we predict an increment of 2.5%/4.1% in Israeli summer daily peak loads toward 2050, and 5.3%/11.6% by the end of century under RCP 4.5/8.5 relative to the baseline scenario, which does not assume global warming. According to the hourly model, the expected effect on summer daily peak loads is more significant than on average daily loads. For winter months, we predict a negative effect on daily peak loads, gradually reaching 3.0%/5.0% by the end of century under RCP 4.5/8.5.

We also show that future annual maximum loads are likely to come from the summer months.

Using temperature simulations downscaled by different IMS stations, we evaluate regional patterns of climate change impact and map spacial effects relative to the country mean.

## השפעת ההתחממות הגלובאלית על הביקוש לחשמל בישראל

טניה סוחוי ומעין טרפר-וכטל

### תקציר

במאמר זה אנו אומדות את השפעת שינויי האקלים הצפויים על הביקוש העתידי לחשמל בישראל. המחקר מבוסס על שני תרחישי התחממות גלובאלית (Representative Concentration Pathway, להלן RCP 4.5 ו-RCP 8.5) הניזונים מסימולציות פרטניות של שינויי אקלים מפרויקט הבין-לאומי CORDEX-AFRICA, אשר השירות המטאורולוגי הישראלי התאים לקואורדינטות והטופוגרפיה של התחנות המטאורולוגיות הקיימות בישראל. במאמר מוצגים לראשונה אומדנים להשפעת שינויי האקלים באמצעות השוואת תחזיות לעומס החשמל המבוססות על תרחישי RCP 4.5/8.5 אל מול תחזיות המבוססות על הטמפרטורות שנצפו בעבר, אשר נבנו בתהליך double-seasonal bootstrap תחת הנחה של העדר מגמת התחממות.

אנו נוקטות בשתי גישות מתודולוגיות: הראשונה מבוססת על פונקציית תגובה (dose response functions) המאפשרת לאמוד, באופן בר-שוואה בין מדינות שונות, את הקשר בין שיאי עומס חשמל יומי לבין הטמפרטורה המקסימאלית באותו יום. אמידות אלו מצביעות על כך שבישראל רגישות הביקוש לחשמל ביחס לטמפרטורה המקסימאלית גבוהה ביחס לאזורים חמים במדינות מפותחות אחרות כגון טקסס ואוסטרליה. הגישה המתודולוגית השנייה משתמשת במודל אקונומטרי לעומס החשמל השעתי בישראל.

בהינתן הרגישות הנוכחית שנמצאה עבור ישראל, תרחישי התחממות RCP 4.5/8.5 צפויים להעלות, עד שנת 2050, את ממוצע שיאי הביקוש היומי לחשמל בחודשי הקיץ ב-2.5%/4.1% מעבר למה שמתקבל מתרחיש של העדר התחממות; עד סוף המאה תוספות אלו צפויות להגיע ל-5.3%/11.6%. לפי המודל השעתי, ההשפעה של ההתחממות על שיאי הביקוש היומי בקיץ משמעותית יותר מההשפעה על הביקוש היומי הממוצע. לעומת זאת, עבור חודשי החורף, ההתחממות הגלובאלית צפויה להביא לירידה בממוצע שיאי ביקוש יומי לחשמל. ירידה זו תגיע, עד סוף המאה, ל-3.0%/5.0% תחת תרחישי RCP 4.5/8.5.

אנו גם מראות שבסבירות גבוהה שיאי הביקוש השנתי לחשמל בעתיד יתרחשו בחודשי הקיץ.

בעזרת סימולציות של טמפרטורות עתידות לפי תחנות מטאורולוגיות בישראל, אנו גם מעריכות את דפוס ההשפעה האזוריים של השינויים האקלימיים, וממפות את ההשפעות האזוריות על עומס החשמל ביחס לממוצע הארצי.

## 1. Introduction

A long-term forecast of electricity demand is a key part of energy infrastructure planning, in light of the rapid privatization of electricity production, the transition to new energy sources (gas, renewable energy sources) and new uses (electric vehicles).

Over the past decade, much empirical work has been devoted to the impact of global warming on electricity demand in the US (Franco and Sanstad, 2008; Deschenes and M.Greenstone, 2011; Auffhammer et al., 2017; Véliz et al., 2017), European countries (Pilli-Sihvola et al., 2010; Wenz et al., 2017; Damm, 2016; Giannakopoulos, 2016), Australia (Ahmed, 2012; Emodi, 2018) and China (Lia et al., 2018; Auffhammer, 2014). The focus was on magnitude, intensity and regional-specific aspects of daily peak loads, regarding their implications on future generation capacity requirements and electrical grid design. Most of these studies, as well as the present work, deal with future climate projections while assuming present technological infrastructure and main consumption patterns.

In Israel, especially after the 21<sup>st</sup> UN Climate Change Conference in Paris in 2015 and the accession of Israel to a global coal reduction agreement, PPCA, in 2018<sup>1</sup>, more attention has been paid to the “mitigation”<sup>2</sup> aspect of climate change, in terms of reducing greenhouse gas emissions, than to the “adaptation” aspect, in terms of managing future demand risks.

This study aims to fill this gap by providing first estimates of climate-related increments in electricity demand and changes in intra-daily load patterns during future decades in Israel.

We derive this climate-induced change using statistical methods, by combining temperature elasticities of demand with future temperature data and assuming existing technology and market fundamentals, thus providing first estimates before the adaptation.

The main inputs for our analysis are high-resolution data on future temperatures generated in the CORDEX project<sup>3</sup> for two emission representative concentration pathways: RCP 4.5 and RCP 8.5,

---

<sup>1</sup> See “The ministries of energy and the environment signed a cessation of coal use by 2030” (Hebrew) -The Marker from 2018, December 17.

<sup>2</sup> See: "Joint press release: Toward a Carbon Pricing Strategy for Israel" from 2020, June 10 concerning the Bank of Israel's proposal for the government to consider imposing a carbon tax - a step that should raise fuel prices for electricity production and electricity prices. URL: <https://www.boi.org.il/en/NewsAndPublications/PressReleases/Pages/10-6-20.aspx>

<sup>3</sup> Coordinated regional downscaling experiment. Most empirical research on the eurozone has been carried out through the EURO-CORDEX data, which also cover Israeli coordinates right on eastern margins of the domain, thus are more prone to extrapolations and distortions. For this reason, further IMS processing was carried out on the CORDEX-AFRICA domain preferred even over the CORDEX MENA domain providing the best Israeli grid but few models to work with.

and further downscaled in the IMS by accounting for retrospective observations from different IMS stations (Climate change report, IMS, 2019). According to this report, the average temperature in Israel rose by about 1.4 C in the period 1950–2017, with the last thirty years making a disproportionately large contribution to this increase; the average temperature in Israel is expected to increase by about 0.9 C from 2018 to 2050 in the optimistic scenario (RCP 4.5) and by 1.2 C in the pessimistic scenario (RCP 8.5); and the recent trend of increasing frequency of hot days and nights and decreasing frequency of cold days and nights is likely to continue. We use temperature simulations for the period up to 2100, available from five global models of the CORDEX project further downscaled by Israeli meteorological stations at hourly frequency, as well as daily maximum temperatures. These data allow us to simulate future loads for each day and hour of the period between 2021 and 2100 and compare their distributions with those obtained without climate change assumption (Suhoy, 2017). We show that the predicted shift upward of winter and summer temperatures will have a greater effect on summer peak loads, adaptation to which will likely require an increase in generation and storage capacity.

We replicate some empirical methods recently applied in the field and contribute to the latest findings with Israeli data. Auffhammer et al. (2017) predict daily peak loads rising more than average loads in the US with the largest (15%) increases in the South and West. Wentz et al. (2017) predict a strengthening of north-south polarization of electricity consumption in Europe under future warming, with a significant decrease in Northern Europe (from -6% to -2% for Sweden and Norway) and an increase in southern and western Europe (from 3% up to 7% for Portugal and Spain), while the current share of renewables is much higher in the north (35.8% in Sweden and 44.8% in Norway) than in the south (Italy 17.6%, Spain 15.2% and Greece 10%); they also predict a shift in annual peak load from winter to summer for 19 of 35 studied European countries. Van Ruijven et al. (2019) suggest that the climate-driven shift in energy demand by 2050 may be more than 25% in the tropics and in the southern regions of the US, Europe and China, but its magnitude will be smaller than the socioeconomically driven increase, which is expected to be the largest in heavily populated tropical developing economies that will only be exposed to modest changes in temperatures. To evaluate the impact of rising temperatures on future electricity demand, Wenz (2017) and Auffhammer et al. (2017) suggest using the dose-response function evaluated for a broad group of countries. This enables us to study a single country that has not yet been exposed to high temperatures, by borrowing the response of other places that have already experienced temperatures beyond their historical range, while controlling for other confounders. We use this approach for a small group of developed countries / load zones that are exposed to high temperatures, like Israel, and have not experienced recent increases in energy demand due to rapid economic growth and/or

changes in technology and income. Besides Israel, we consider five states of Australia, operated by the NEM power system, and eight load zones of Texas, operated by the ERCOT.

Our results-based retrospective data for the selected group of countries provide evidence that the Israeli sensitivity to temperatures is much higher than the median response in the group. We project future Israeli daily peak loads by daily maximum temperatures up to 2100, based on CORDEX downscaled data, while assuming the current (high) and the lower (median) level of sensitivity. Note that a discussion of socioeconomic, demographic, and technological factors of baseline electricity demand is beyond the scope of this study.

Using CORDEX simulations, we are also able to evaluate intra-daily effects of warming scenarios based on hourly temperatures provided by the IMS up to 2100. Here we employ the MEFM forecasting equations of R. Hyndman (2015), previously applied by Suhoy (2017) in constructing a long-run probabilistic forecast of peak electricity demand in Israel. We document a greater incremental change in demand for off-peak summer hours. We show also that future annual peaks are likely to come from the summer periods under both RCP scenarios.

The paper is organized as follows: The next section describes the data. The third section summarizes indicators of the temperature sensitivity of electricity demand based on the load curve characteristics of selected countries/load zones, and provides estimated impacts of global warming on daily peak loads based on evaluated dose-response functions. The fourth section deals with intra-day changes and provides first estimates of a possible shift in annual maximum peak distribution based on an hourly model. The fifth section concludes.

## **2. The data**

Retrospective high-frequency data on electricity consumption, daily maximum temperatures and holidays for each country/state were downloaded from the corresponding official sites. Appendix A (Table A1) provides further details. CORDEX simulations of daily maximum temperatures of Texas and Australia were downloaded from the CORDEX North America and Australasia domains, using coordinates corresponding to the major cities of selected load zones to make sure that our results are in line with those of Auffhammer et al. (2017) and Emodi (2018).

The Electricity Authority provided hourly data of electricity production in Israel from 2002. Further updates are now available from the Israel Electric Corporation (IEC) website.

Retrospective data of daily maximum and hourly temperatures and relative humidity were downloaded from the Israeli meteorological database ([ims.data.gov.il](http://ims.data.gov.il)), by station. Future

temperature projections made upon Israeli coordinates are available until 2100 from a number of global models participating in Coupled Model Intercomparison Project – Phase 5 (CMIP5) and providing simulations for the CORDEX-AFRICA domain with a grid of about 50 km. These temperature simulations were downloaded by IMS and statistically downscaled with regard to homogenized historical by-station observations.<sup>4</sup> Thus, this study employed daily maximum temperature and hourly temperature forecasts for the period between 2021 and 2100 from 5 CORDEX models, processed by IMS. Table A2 (Appendix A) provides further details, as well as a list of the CMIP5 models used. Table A3 (Appendix A) lists IMS stations with downscaled data provided and maps these stations into corresponding District (Nafa) and meteorological polygons, which are further used in our analysis of regional impacts.

The macroeconomic forecasts of future GDP growth and population, used in this study for estimating seasonal mean demand as a low-frequency component of hourly electricity demand projections, are from Argov and Tsur (2019).

### **3. Temperature sensitivity and estimated dose-response functions**

#### **3.1. Load curve shapes in the selected group**

Table 1 presents the selected load zones, their size, and the occurrence of annual peak load in summer months, as observed in the past two decades. As can clearly be seen in the third column, the probability of the annual peak load occurring in the summer exceeds 70% for 12 of the 14 locations considered.

Intra-daily load patterns differ between countries, first, due to different ranges of temperatures, and second, due to different sensitivities of electricity demand to these temperatures.

Figures 1–3 depict daily load curves for Israel, NEM (Australia) and ERCOT (Texas) load systems, displayed as deviations of hourly loads from the corresponding seasonal mean<sup>5</sup> over the period from 2003 to 2019 in the summer months (from April to September in Israel and Texas, and from October to March in Australia). The graphs show a great deal of similarity between load patterns of the selected "hot" zones, with the mean and variance of the load deviations increasing as we move to higher temperature ranges, and the intra-percentile peak loads correspond to the hours when daytime temperatures reach their maximum. It can be seen that the Australian load curves have a smaller range of variation than the Israeli and Texas ones, and the latter develop similar

---

<sup>4</sup> With Quantile Delta method applied. Further details on the IMS downscaling are available (in Hebrew) from the Climate Change Report, IMS, 2019, Statistical Downscaling Appendix.

<sup>5</sup> Calculated as quarterly (three-month) averages of actual loads, by hour.

amplitudes to the Israeli curves at much higher temperatures on the upper percentiles. We will discuss this point in more detail below.

**Table 1: Population (2019) and occurrence (%) of the annual maximum load over the period 2002–19, by selected countries/states/load zones**

	Population <sup>a)</sup> (2019, thousands)	Occurrence (%) of the annual peak		
		In Summer <sup>b)</sup>	In the interval	
			12:00 - 15:00	16:00 - 19:00
<b>Panel A. Australia</b>	<b>25364</b>			
New South Wales	8090	60		100
Queensland	5095	100	50	50
South Australia	1752	100	10	90
Tasmania	534	50	50	50
Victoria	6595	100	30	70
<b>Total NEM</b>	<b>22065</b>	<b>60</b>	<b>5</b>	<b>95</b>
<b>Panel B. Israel - total</b>	<b>8972</b>	<b>74</b>	<b>78</b>	<b>22</b>
<b>Panel C. Texas</b>	<b>29000</b>			
Coast	7508	100	94	6
South	1641	83	94	6
South Central	8126	100	41	59
West	399	100	89	11
Far West	478	100	100	
North Central	7273	100	78	22
East	342	94	82	18
North	335	100	94	6
<b>Total ERCOT</b>	<b>26100</b>	<b>100</b>	<b>94</b>	<b>6</b>

a) Population numbers in ERCOT load zones have been approximately estimated proportional to the size of main cities in the corresponding areas.

b) Summer months in Israel and Texas are defined from April to September, for Australia – from October to March.

Generally, flatter load curves indicate electricity demand that is less prone to change throughout the day as a result of lower dispersion of temperatures or behavioral factors and therefore has fewer power fluctuations, avoids overloads in parts of the system, requires less regulating capacity and has smaller transmission costs. Load curves may be flattened by differentiation of electricity tariffs

between peak and off-peak hours, through economic dispatching<sup>6</sup> and through transitioning to renewable energy.

To compare the shapes, we consider below (Figure 4) the main load curve characteristics<sup>7</sup>, defined as follows:

- the evolution of the average log-difference between daily mean and maximum loads over the summer months, from 2010 to 2019, by country;
- the evolution of the average log-difference between daily minimum and maximum loads over the summer months, from 2010 to 2019, by country;
- the evolution of the ramp rate factor, defined as the mean absolute change in load relative to the maximum load (in log-difference terms), calculated daily and averaged over the summer months, from 2010 to 2019, by country.

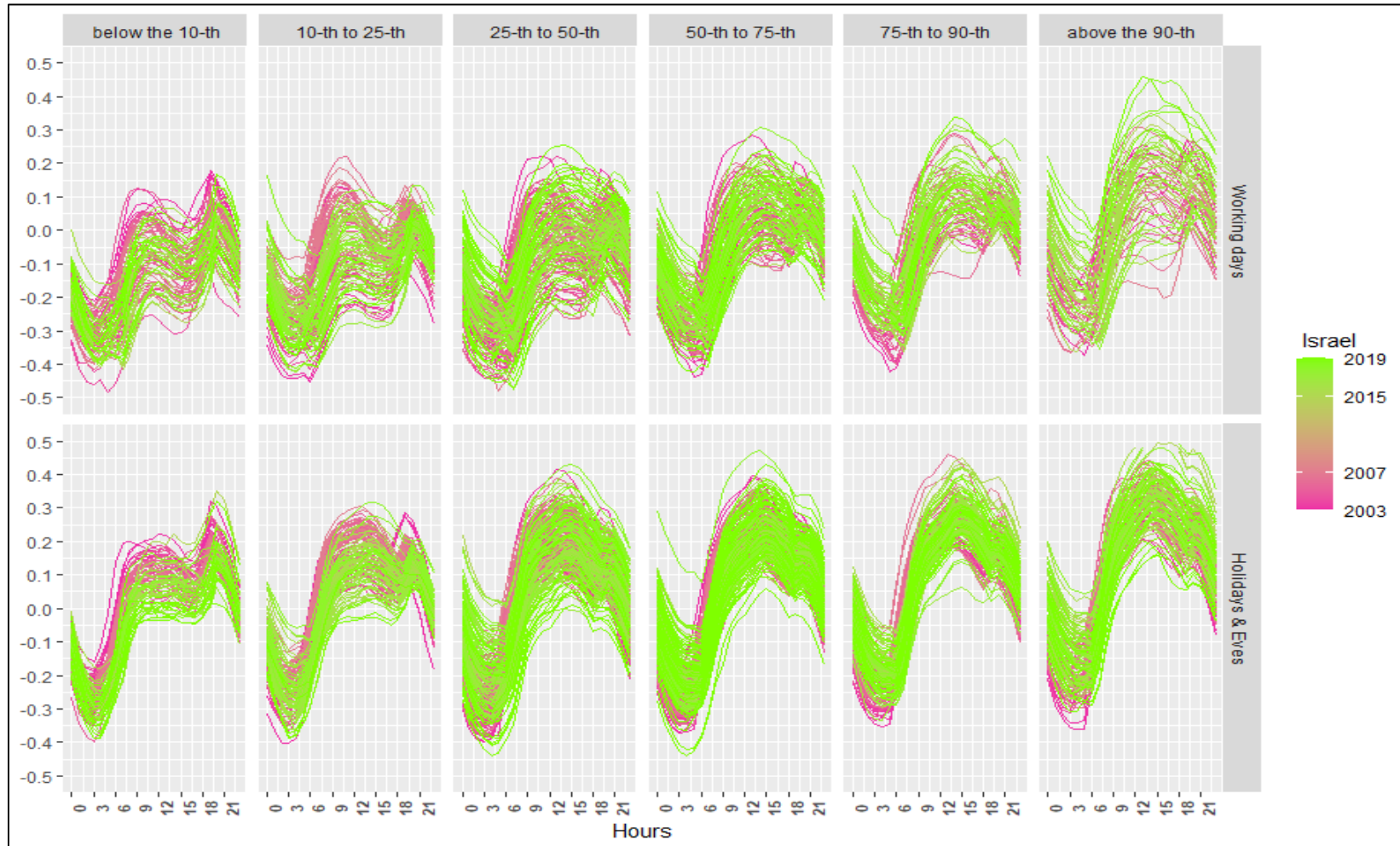
Indicators of max/mean and max/min load ratios presented in Figure 4 provide further evidence of flatter load shapes in Australia, likely due to extremely flexible intra-day pricing, which is transparent and available to the public through a website, thus allowing planning and optimization of electricity use on each particular day. According to these ratios, Texas load curves develop a greater magnitude, compared to Israeli ones, due to higher summer temperatures observed beyond the Israeli range. The graphs on the right side show a gradual decrease of the Ramp Rate Factors of loads in Israel and Texas over the period of 2003 to 2019, thus providing an indication of flattening.

---

<sup>6</sup> 2011/2012 and 2013 Economic Dispatch and Technological Change. - U.S. Department of Energy Report to the Congress. This report considers the main aspects of economicDispatch, as following: generation resources, energy storage, the production tax credit, market structure, environmental regulations, demand response market power and stresses the need for grid flexibility which uses price signals and technology advances and ensures that the lowest cost resources are dispatched first.

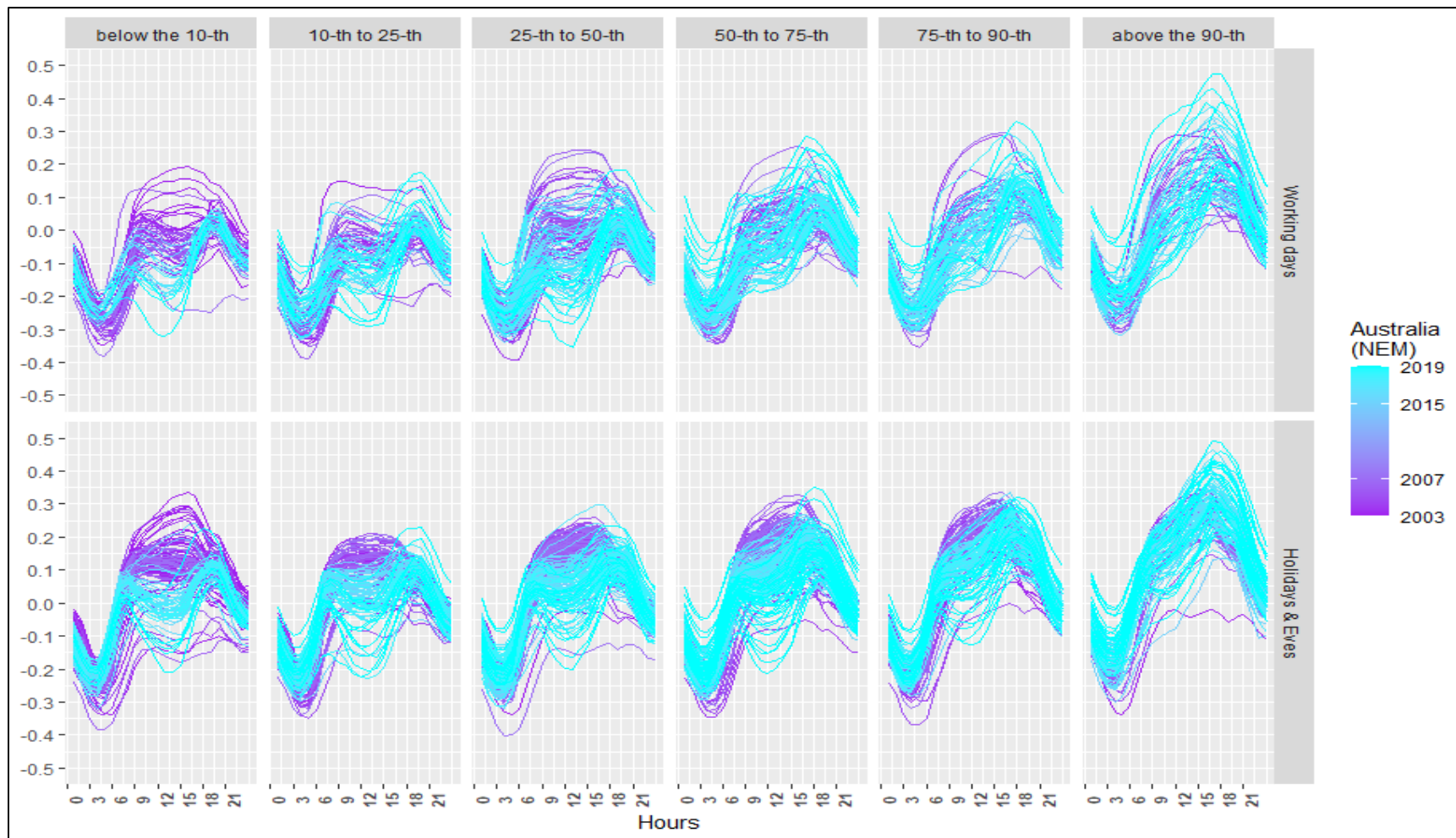
<sup>7</sup> For details see: Neagu et al. (2011) and Bobmann, T. and I. Staffel (2015) “The Shape of Future Electricity Demand: Exploring Load Curves in 2050s Germany and Britain” – URL: <http://dx.doi.org/10.1016/j.energy.2015.06.082>

**Figure 1: Daily load curves<sup>a)</sup> of Israel in summer months (April-September), by daily maximum temperature percentiles, during the period 2003–19**



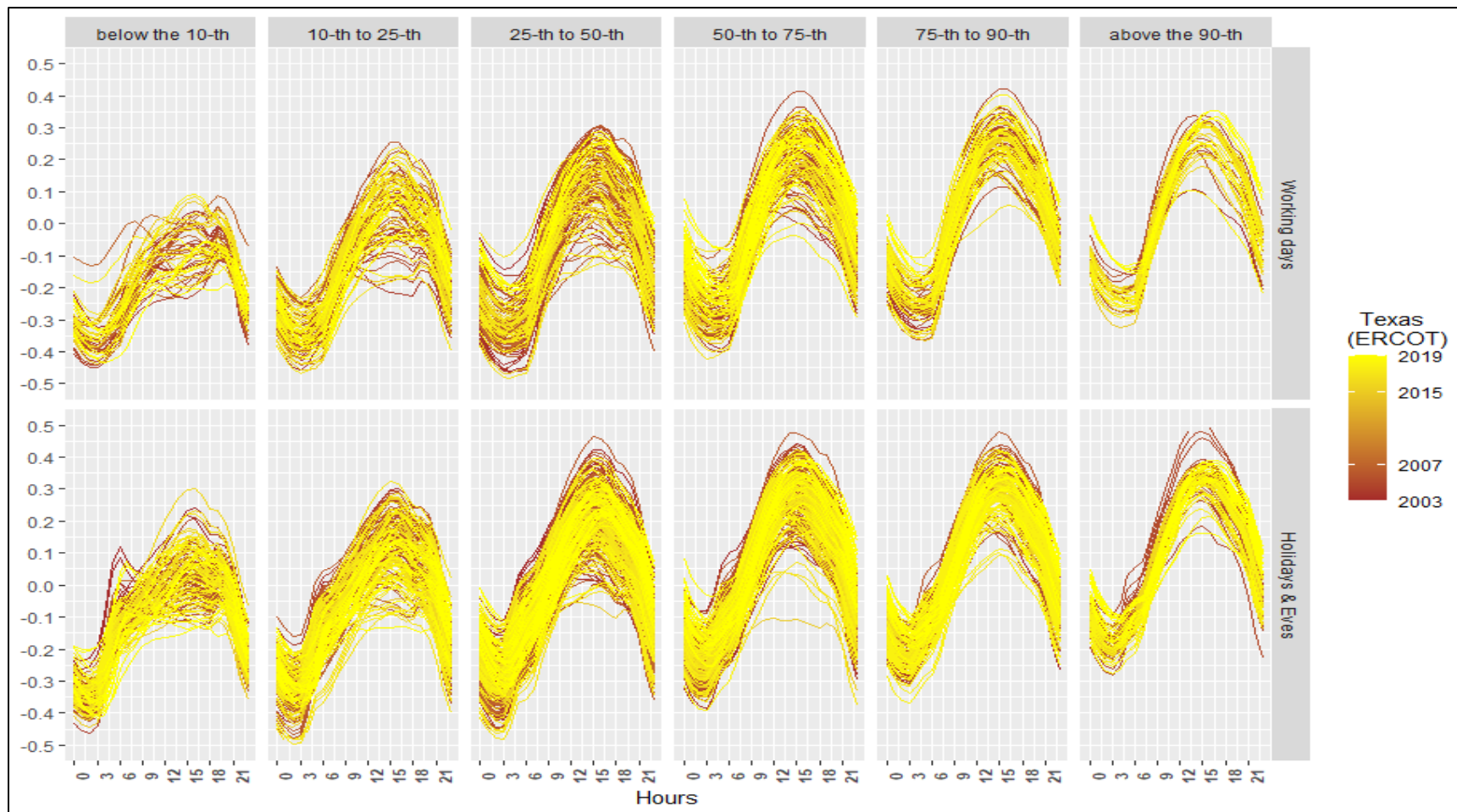
<sup>a)</sup> In terms of log-deviations from the quarterly means

**Figure 2: Daily load curves<sup>a)</sup> of the NEM system (Australia) in summer months (October-March), by daily maximum temperature percentiles, during the period 2003–19**



<sup>a)</sup> In terms of log-deviations from the quarterly means

**Figure 3: Daily load curves<sup>a)</sup> of the ERCOT system (Texas) in summer months (April-September), by daily maximum temperature percentiles, during the period 2003-2019**



<sup>a)</sup> In terms of log-deviations from the quarterly means

Table 2 summarizes changes occurring in these characteristics between the periods 2003–07 and 2015–19, and also provides data on the average duration of load remaining above 75% and 90% of annual peak during 2015–19, which allow additional between-country comparison. As can be seen, the decrease in the Max to Min ratio of daily loads in Workdays is the most indicative in terms of flattening of load curves that has occurred in all three countries, although Max/Average ratios for Australia have moved in opposite directions since 2013.

**Table 2: Changes<sup>a)</sup> in load curve characteristics in summer months<sup>b)</sup>, 2015–19 vs. 2003v07), and average duration (in hours) of loads remaining above 75% and 90% of annual peak in 2015–19, by selected countries/zones and working/non-working days**

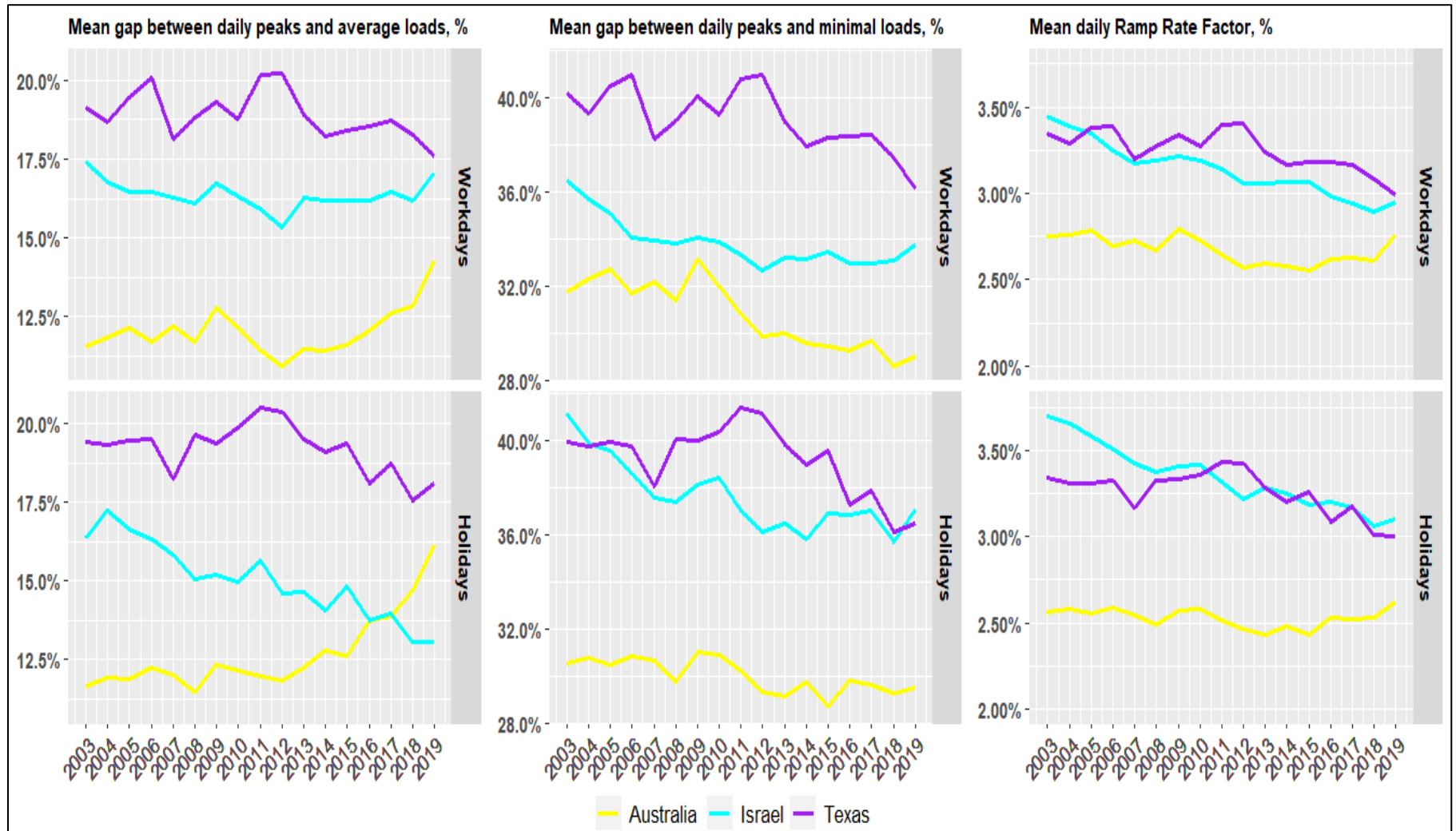
	Change <sup>a)</sup> in Max/Ave load ratio		Change <sup>a)</sup> in Max/Min load ratio		Change <sup>a)</sup> in Ramp Rate Factor		Duration (hours) of load remaining above:			
							75% of Max		90% of Max	
	Workdays	Holidays	Workdays	Holidays	Workdays	Holidays	Workdays	Holidays	Workdays	Holidays
<b>Panel A. Australia</b>										
New South Wales	0.1%	1.5%	-5.2%	-2.5%	-0.2%	-0.2%	6.16	4.45	3.04	3.22
Queensland	1.6%	2.7%	-7.2%	-4.9%	-0.4%	-0.4%	7.28	5.52	5.26	5.19
South Australia	3.8%	7.7%	0.3%	14.0%	0.8%	0.9%	5.24	5.42	3.41	2.67
Tasmania	-0.4%	-0.4%	-2.7%	-2.1%	0.1%	0.0%	9.06	6.87	3.54	2.49
Victoria	3.3%	5.6%	5.7%	7.5%	0.3%	0.3%	4.81	6.35	4.33	5.13
<b>Total NEM</b>	<b>0.6%</b>	<b>2.9%</b>	<b>-4.7%</b>	<b>-1.6%</b>	<b>-0.1%</b>	<b>-0.1%</b>	8.74	4.76	3.04	3.22
<b>Panel B. Israel</b>										
<b>Total</b>	<b>-0.3%</b>	<b>-1.8%</b>	<b>-3.8%</b>	<b>-2.0%</b>	<b>-0.4%</b>	<b>-0.3%</b>	<b>9.13</b>	<b>7.22</b>	<b>4.04</b>	<b>3.75</b>
<b>Panel C. Texas</b>										
Coast*	0.6%	1.8%	1.1%	3.0%	0.0%	0.1%	9.48	8.73	4.47	4.35
South*	0.1%	0.5%	-0.8%	-0.3%	-0.1%	0.0%	9.32	8.56	4.53	4.19
South Central*	0.1%	0.2%	-1.8%	-0.8%	-0.1%	-0.1%	7.90	7.51	4.32	4.40
West*	-2.2%	-1.6%	-8.2%	-6.6%	-0.5%	-0.4%	8.23	8.13	4.22	3.91
Far West*	-5.4%	-4.4%	-12.7%	-10.7%	-0.8%	-0.7%	14.37	14.06	6.14	5.83
North Central*	-1.3%	-0.4%	-5.4%	-2.7%	-0.3%	-0.1%	8.03	7.56	4.50	4.54
East*	-0.1%	0.3%	-1.5%	-0.6%	-0.1%	0.0%	8.76	8.04	4.55	4.21
North*	-4.2%	-3.8%	-13.1%	-11.6%	-0.7%	-0.6%	8.50	7.76	4.49	4.37
<b>Total ERCOT</b>	<b>-1.2%</b>	<b>-0.3%</b>	<b>-4.1%</b>	<b>-1.7%</b>	<b>-0.2%</b>	<b>-0.1%</b>	<b>9.14</b>	<b>8.50</b>	<b>4.69</b>	<b>4.57</b>

a) Negative changes in Max/Average, Max/Min ratios and Ramp rate factor indicate flattening load curves.

b) Summer months in Israel and Texas are defined from April to September, for Australia – from October to March.

In the next sub-section we show that Israeli load sensitivity relative to temperature is the highest among the countries surveyed, meaning demand for electricity in response to high temperatures experiences a sharper increase in Israel than in the other countries when faced with a similar temperature high. This finding is in accordance with the findings in this section regarding the shape of Israel's load curve.

**Figure 2: Load curve characteristics in summer months during the period 2010–19, by country**



### 3.2. Estimated dose-response functions

Dose-response function estimation was applied by Wenz et al. (2017) and Aufhammer et al. (2017) while estimating regional distribution of climate-induced shifts in electricity demand for European countries and, separately, for US states. It estimates country-specific U-shape dependencies of peak/average daily loads on 2% trimmed daily maximum temperatures over retrospective data, while the non-temperature effects of low-frequency-factors (socioeconomic, demographic, and technological) are captured globally through Chebyshev polynomials and calendar dummies, and then removed (B.2). Normalizing these results to the load ranges of individual countries makes the residual loads comparable, enabling the construction of a common response function and the projection of future loads outside the range of temperatures observed in the retrospective of a single country (B.3). Using this approach, we combine Israeli data with data collected from the National Electricity Market (NEM) providing electricity for 5 states of Australia and data from 9 Texas load zones operated by the Electricity Reliability Council of Texas (ERCOT).

Appendix B provides a technical description of this method. Appendix C reports the main country/state-specific parameters and results of regression (B.1).

Figure 3 presents estimated U-dependencies of non-normalized daily peak loads on 2% trimmed daily maximum temperatures, adjusted for macroeconomic, seasonal, and calendar factors, estimated for Israel and for each state or load zone in Australia and Texas through (B.2).

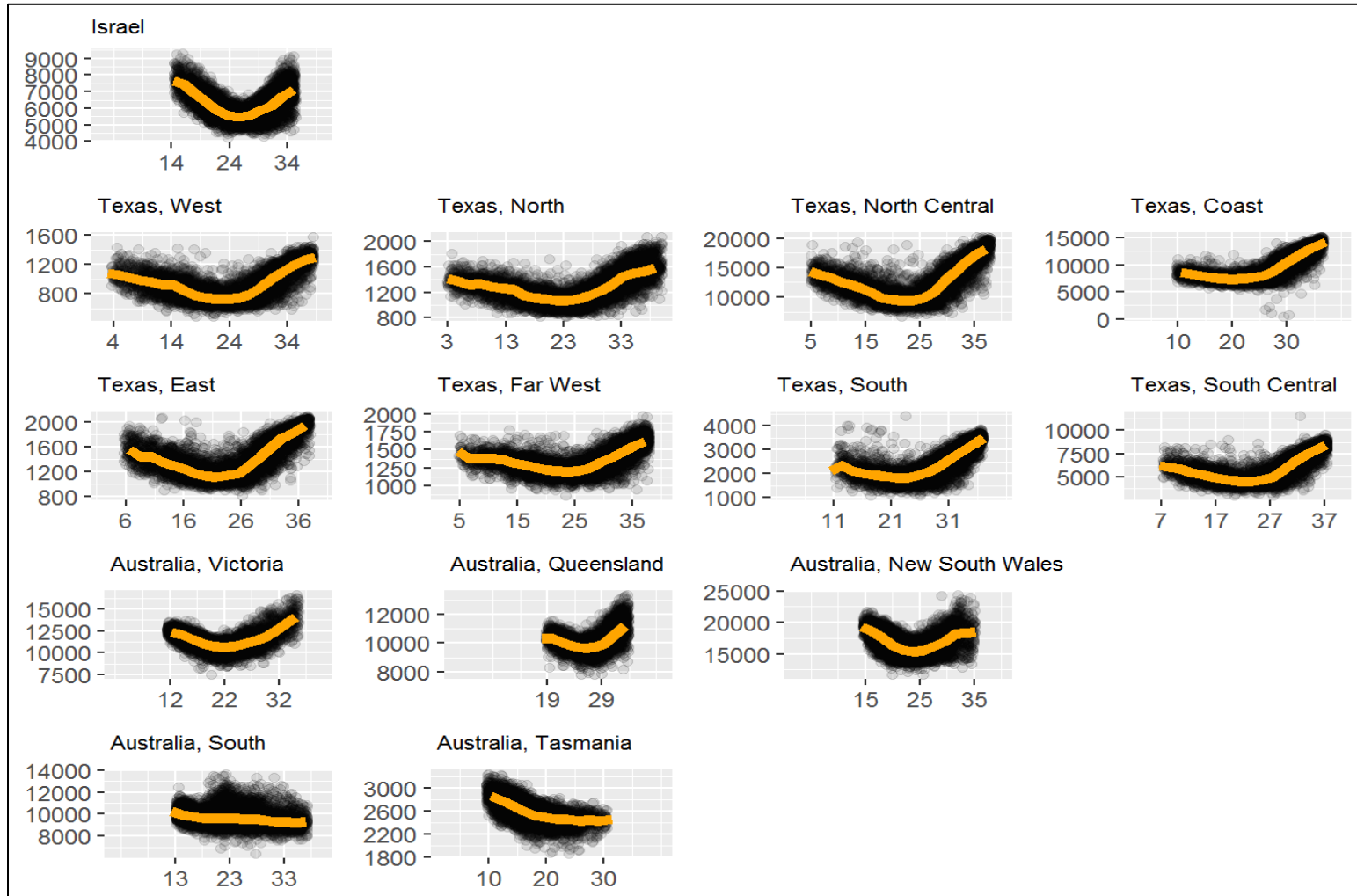
Figure 4 depicts the common response, calculated from the normalized loads (B.3) across all zones. As can be seen from Figure 4, the common dose-response function implies a lower sensitivity to temperatures than could be obtained using only Israeli data. In order to provide a comparison of Israeli retrospective data, projected through the common and Israeli-specific dose-response curves, we employ back-transformation (B.4) and show both versions in Figure 5, while the higher sensitivity of Israeli peak loads becomes even more evident.

Assuming that the sensitivity of future daily peak loads to maximum daily temperatures remains at the current level, we make our projections using IMS data up to 2100 from all five models—by RCP 4.5 and 8.5—and compare these results with forecasts based on double-season-block bootstrap of actual temperatures observed since 2002<sup>8</sup> (baseline scenario levels assuming no global warming trend).

---

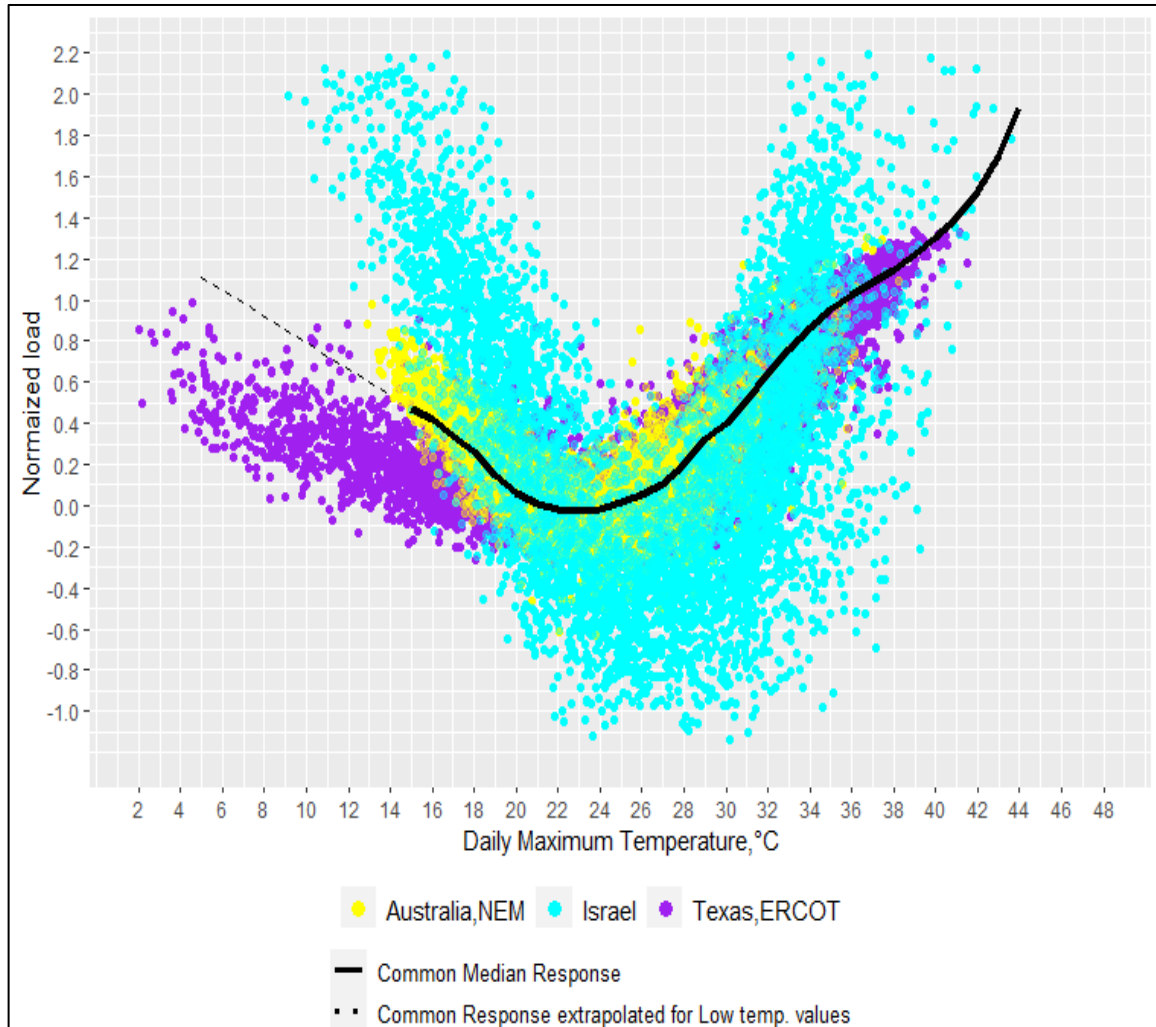
<sup>8</sup> For details see Hyndman and Fan (2015).

**Figure 3: Country/state/load zone-specific load dependencies on daily maximum temperatures ( $^{\circ}\text{C}$ ), estimated by daily data (2002-2019) <sup>a)</sup>**



<sup>a)</sup> The horizontal axis is  $^{\circ}\text{C}$  with a range determined by local conditions. The black dots represent daily peak loads (the vertical axis) in each country/state/load zone, adjusted for low-frequency and calendar effects. The orange line is the median load for temperature bins of  $1^{\circ}\text{C}$  width connected linearly.

**Figure 4: Common response function <sup>a)</sup>**



<sup>a)</sup> Estimated on daily peak loads recorded in Israel, NEM (Australia) and ERCOT (Texas) between 2002 and 2019, and corresponding daily maximum temperatures. Disaggregated data for the Australian states (excluding South Australia and Tasmania whose data don't provide evidence of U-shaped response) or ERCOT's load zones give similar results, but with a larger noise component

Table 3 presents mean bootstrapped differences (in %) between daily peak per-capita loads forecasted under different RCP-scenarios and under the baseline scenario of no global warming trend. The top panel of this table presents results calculated through high-sensitivity response function, and the bottom panel is through low-sensitivity (common) response function.

As shown, the main effect of rising temperatures on daily peak per-capita loads appears in summer seasons. Using the high-sensitivity function, we can expect an increase of 2.5% /4.1% by 2050-2060 and of 5.3% / 11.6% toward 2100, according to RCP 4.5/8.5 temperature data.

**Table 3: Estimated impact of future global warming on peak daily loads, by sensitivity assumption, RCP scenario and decade** <sup>a), b)</sup>

		<b>RCP 4.5</b>		<b>RCP 8.5</b>	
<b>High (current) sensitivity scenario</b>					
<b>Panel A. Summer</b>					
2020-2030	-0.33	[ -1.03	, 0.52 ]	1.23	[ 0.51 , 2.04 ]
2030-2040	1.90	[ 1.01	, 2.55 ]	2.69	[ 2.02 , 3.55 ]
2040-2050	2.05	[ 1.23	, 2.91 ]	3.81	[ 2.71 , 4.18 ]
2050-2060	2.45	[ 1.87	, 3.66 ]	4.06	[ 3.24 , 5.22 ]
2060-2070	3.58	[ 2.45	, 4.23 ]	5.49	[ 4.37 , 6.73 ]
2070-2080	4.39	[ 3.55	, 5.28 ]	8.13	[ 6.48 , 10.72 ]
2080-2090	5.01	[ 4.05	, 6.08 ]	10.07	[ 8.65 , 12.44 ]
2090-2100	5.33	[ 4.25	, 6.51 ]	11.57	[ 9.26 , 13.18 ]
<b>Panel B. Winter</b>					
2020-2030	0.21	[ -0.02	, 0.43 ]	-0.12	[ -0.34 , 0.21 ]
2030-2040	0.15	[ -0.12	, 0.45 ]	-0.32	[ -0.56 , 0.09 ]
2040-2050	-0.18	[ -0.45	, 0.08 ]	-0.67	[ -1.14 , -0.08 ]
2050-2060	-1.86	[ -2.36	, 0.62 ]	-2.02	[ -3.13 , -1.14 ]
2060-2070	-2.32	[ -3.01	, -1.60 ]	-3.02	[ -4.07 , -2.07 ]
2070-2080	-2.51	[ -3.13	, -1.95 ]	-4.12	[ -5.29 , -3.25 ]
2080-2090	-2.98	[ -3.75	, -2.08 ]	-4.98	[ -6.01 , -3.40 ]
2090-2100	-3.02	[ -4.02	, -2.19 ]	-5.03	[ -6.51 , -3.93 ]
<b>Low (median) sensitivity scenario</b>					
<b>Panel A. Summer</b>					
2020-2030	-0.09	[ -0.53	, 0.17 ]	0.24	[ 0.02 , 0.53 ]
2030-2040	0.63	[ 0.30	, 1.14 ]	0.80	[ 0.54 , 1.11 ]
2040-2050	0.96	[ 0.59	, 1.81 ]	1.28	[ 1.07 , 2.02 ]
2050-2060	1.73	[ 1.19	, 2.33 ]	1.84	[ 1.22 , 2.31 ]
2060-2070	2.38	[ 1.88	, 2.68 ]	3.10	[ 2.45 , 3.50 ]
2070-2080	2.68	[ 2.05	, 3.14 ]	3.50	[ 3.02 , 4.00 ]
2080-2090	2.85	[ 2.25	, 3.42 ]	4.50	[ 4.01 , 5.56 ]
2090-2100	3.01	[ 2.67	, 3.86 ]	4.98	[ 4.15 , 6.08 ]
<b>Panel B. Winter</b>					
2020-2030	0.33	[ 0.04	, 0.37 ]	0.57	[ 0.26 , 0.14 ]
2030-2040	0.18	[ 0.04	, 0.27 ]	0.23	[ 0.03 , 0.39 ]
2040-2050	-0.32	[ -0.17	, -0.06 ]	-0.14	[ -0.21 , -0.05 ]
2050-2060	-0.06	[ -0.13	, 0.03 ]	-0.25	[ -0.37 , -0.08 ]
2060-2070	-0.08	[ -0.12	, -0.03 ]	-0.23	[ -0.32 , -0.05 ]
2070-2080	-0.19	[ -0.22	, -0.06 ]	-0.58	[ -0.76 , -0.39 ]
2080-2090	0.04	[ -0.03	, 0.10 ]	-0.64	[ -0.86 , -0.46 ]
2090-2100	-0.02	[ -0.04	, 0.09 ]	-0.70	[ -0.92 , -0.48 ]

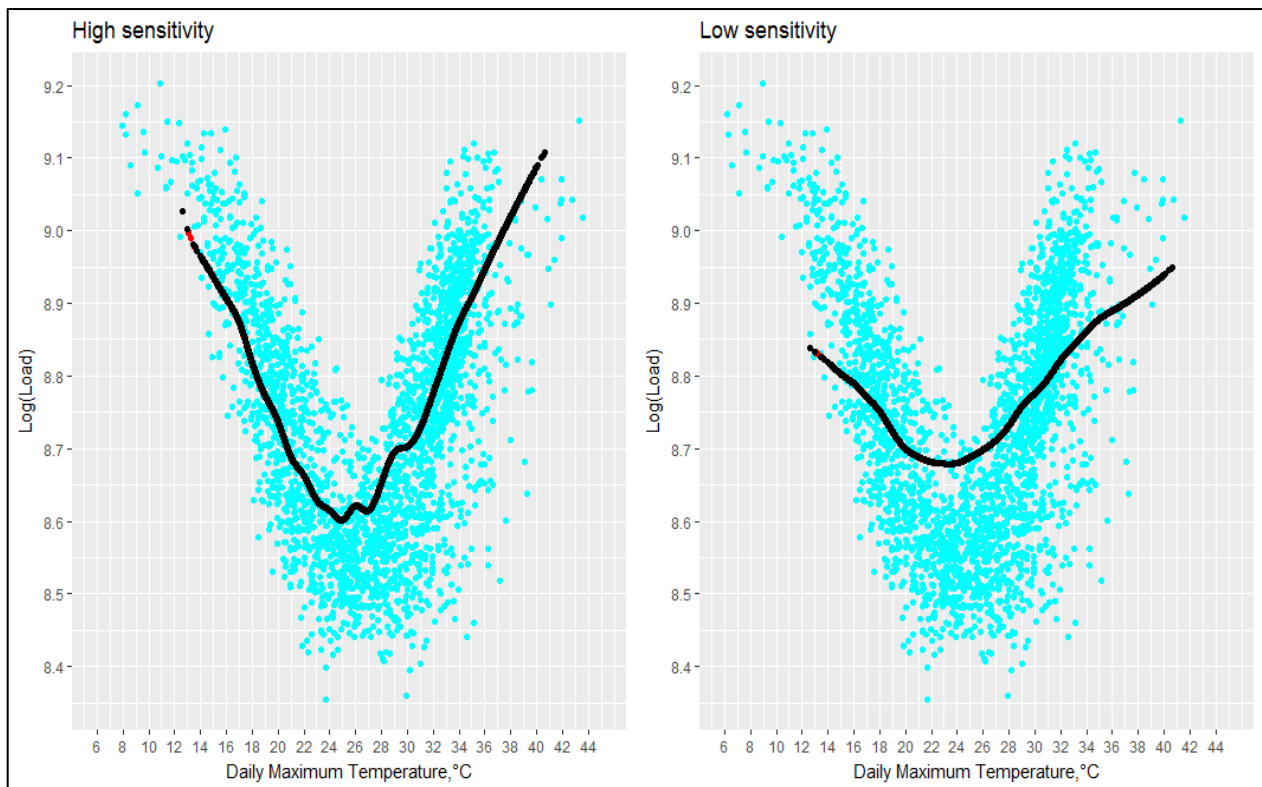
<sup>a)</sup> Relative to baseline scenario daily peak loads, adjusted for low-frequency factors and calendar effects and assuming no global warming trend. The first column of each RCP scenario reports the mean change and the numbers in brackets report the 5% and 95% percentiles of the distribution of bootstrapped differences. Future daily peak loads are projected through the common dose-response function.

<sup>b)</sup> Future daily maximum temperature data are CORDEX-AFRICA simulations, downscaled by the IMS according to five different models (see Appendix B).

For winter seasons, a non-significant/small decrease was obtained by 2050-60 under RCP 4.5/8.5 and a decrease in daily peaks of 3.0%/5.0% was suggested by the high-sensitivity scenario toward the end of the century under RCP 4.5/8.5. The low-sensitivity response function does not reveal significant changes in summer daily peaks by the middle of the century and an increase of 3.0%/4.98% by the end of the century under RCP 4.5/8.5. No significant changes in winter daily peak loads were detected with the low-sensitivity function.

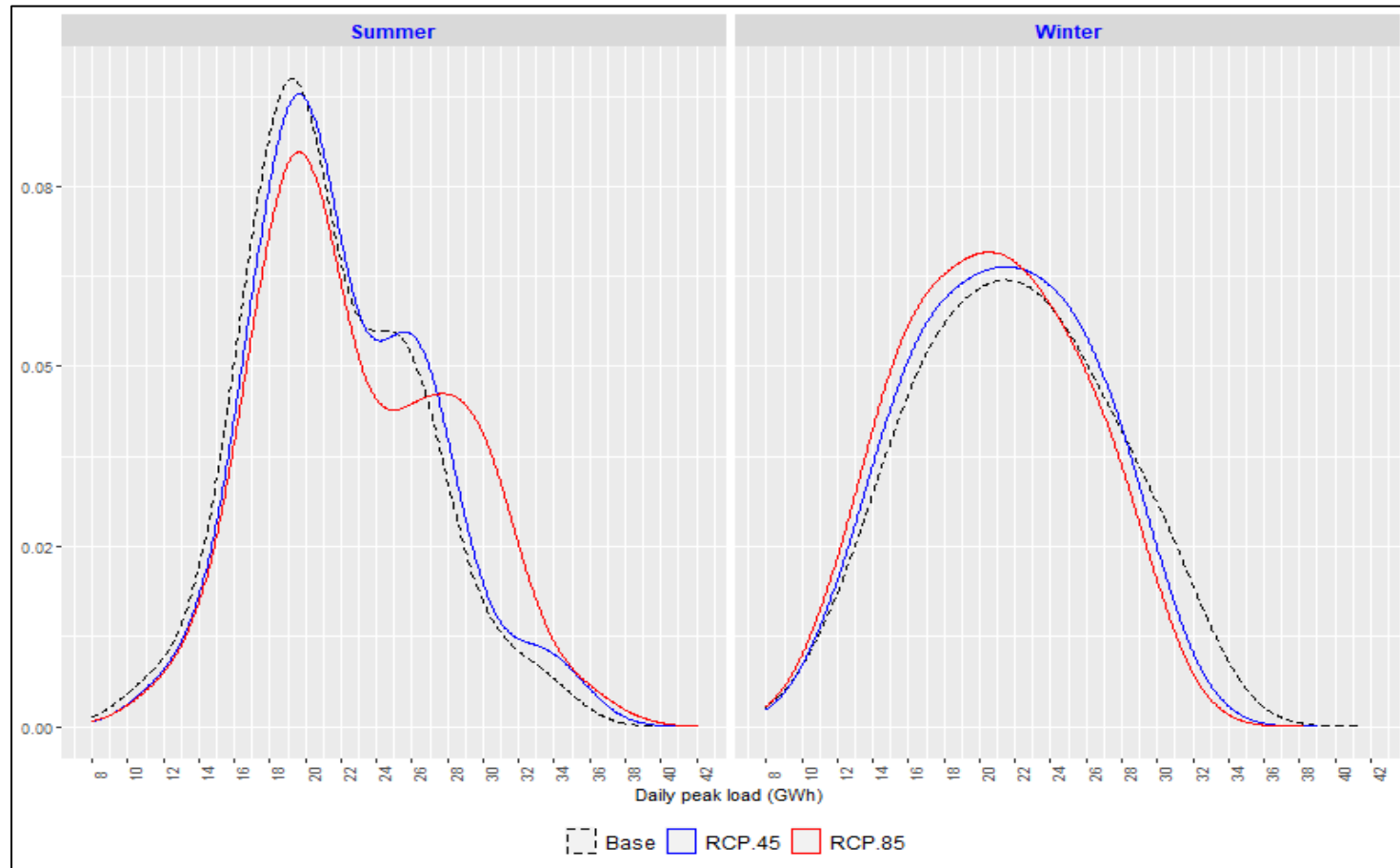
It is interesting to compare our results with those reported by Auffhammer (2017) for the ERCOT system (Texas), exposed to temperatures beyond the Israeli range. This study evaluates an increase in daily peak loads of 4.3%/11.5% by the end of century, under RCP 4.5/8.5.

**Figure 5: Daily peak loads <sup>a)</sup> of Israel, projected retrospectively (2002–19) by daily maximum temperatures through Israeli-specific (high sensitivity, left) and common response (low sensitivity, right) functions**



<sup>a)</sup> In log terms. Blue dots denote actual data adjusted for low-frequency and calendar effects using (D.2). The solid black lines show back-projected loads, estimated through high-sensitive and common response functions.

**Figure 6: Distributions<sup>a)</sup> of daily peak loads predicted for the period 2041–60 under the baseline (of no global warming) and different RCP scenario (4.5 and 8.5), by season**



<sup>a)</sup> Shown are kernel density plots of daily peak loads, predicted by daily maximum temperatures simulated basing on presently observed data (the baseline) or by future temperature data simulated from 5 IMS models assuming RCP 4.5 and 8.5 scenarios. Since our model is estimated with regard to per-capita loads, the average forecast of the Israeli population between 2041 and 2060 was used to provide density forecasts in terms of overall daily peak loads.

Figure 6 depicts forecasted distributions of daily peak loads, projected with an assumption of high sensitivity response. These use daily maximum temperature simulations from five IMS models for the period between 2041 and 2060, compared to the baseline forecasts assuming no global warming trend, based on the hourly model of Hyndman and Fan (2015). To enable transition from per-capita loads, as estimated by the model to overall load forecasts, we use the average forecast of Israeli population between 2041 and 2060.

As follows from Figure 6, densities of daily peak loads obtained for summer months between 2041 and 2060 are bimodal and shift to the right under both RCP-scenarios compared to the baseline. For winter months there is a small shift of the probability mass to the left. As shown in the next section, the impact of rising temperatures on summer daily peak loads is almost twice as large as on average daily loads.

Figure 7 presents the predicted incremental differences between the Israeli average and simulations based on regional data. Predictions for stations were made using the same (high-sensitive) dose-response function as the general Israeli predictions, while using station data for both RCP scenarios. The IMS recently defined 23 natural meteorological regions in Israel, to which we attributed the mean incremental difference of the stations within the area.

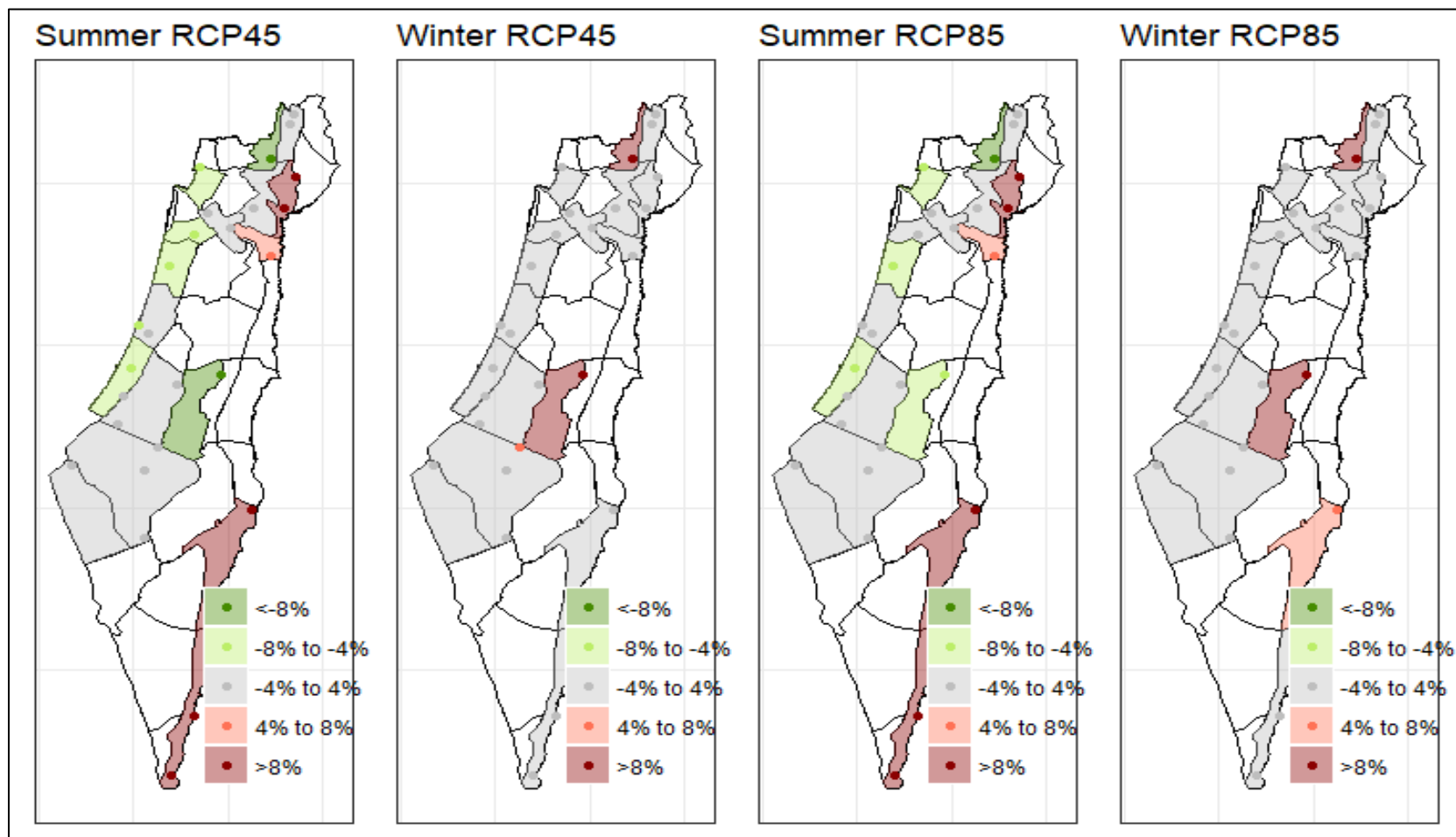
Relative to the country average effect, we find lower incremental increases in hillier and cooler regions during summer months, and higher incremental increases in in the warm regions of the country. Regions with no representing stations were left blank.

#### **4. Estimated impacts based on hourly temperature projections**

Having estimated the parameters of twenty-four hourly regressions (D.1-D.2) using 2002–19 data, we can now make projections for future loads, given long-run forecasts of GDP and population growth, as well as our assumptions about temperature trends. Note that here we are dealing with the high-sensitivity response, as the parameters are based only on retrospective Israeli data.

As shown in Appendix D, our projections of electricity demand for each hour heavily depend on temperature data, first, through its low-frequency component, which includes an effect of the number of heating and cooling days in each quarter and second, through the high-frequency component that includes a non-linear effect of hourly temperatures.

Figure 7: Regional effects of temperature changes relative to the mean-country effect <sup>a)</sup>, estimated by 2050–60 under RCP 4.5 and 8.5



a) In terms of increase (+) / decrease (-) relative to country mean, %.

Therefore, the estimated impact of global warming-based hourly loads builds on the following temperature inputs. One is CORDEX simulations of daily maximum temperatures, downscaled by IMS according to five different models (Appendix A, Table A2), which enable us to obtain the number of cooling and heating days in each future quarter, affecting predicted seasonal mean levels under RCP 4.5 and 8.5 scenarios. For the baseline, we use bootstrapped historical counts of cooling and heating days, by quarter. The second input is CORDEX simulations of hourly temperatures, downscaled and available by five different models, which allow us to evaluate hourly deviations (in log terms) from projected seasonal mean levels to be compared with the baseline deviations, assuming no trend in future temperatures; the baseline deviations have been simulated using double-seasonal bootstrap of historical temperature values, as described in Hyndman and Fan (2015).

The residuals for both baseline and RCP scenarios were simulated using the ACF detected upon historical hourly loads and appropriately bootstrapped. To evaluate the impact over a selected fraction of hours or days, we compare the corresponding loads, projected under each RCP scenario vs. the baseline and bootstrap the differences, thus providing the mean difference, as well as its 5% and 95% percentiles.

We also evaluate an expected shift in the distribution of annual peak load, as well as possible changes in its shape under both RCP scenarios.

Table 4 reports bootstrapped changes in average summer loads relative to the baseline forecast obtained for the same days. For summer months of the 2051–60 decade, the results indicate an increase in average electricity demand of 1.8% / 3.1% compared to the 2.7% / 4.6% increment obtained for daily peak loads under RCP 4.5 / RCP 8.5, respectively, for the same period. Note that the impact on daily peak loads evaluated from the hourly model is very close to the shift obtained for this decade from the dose-response function (see the previous section).

Having in hand hourly simulations of loads, projected until 2100 under the baseline and two RCP scenarios, we are also able to focus on some tail-characteristics that matter for capacity planning. Table 5 reports frequencies of hours (Panel A) and daily peaks (Panel B) exceeding the current<sup>9</sup> 90th / 95th percentiles of per-capita electricity demand, simulated for summer months between 2041–60 and between 2081–2100 under the baseline RCP 4.5 and RCP 8.5 scenarios.

---

<sup>9</sup> As a benchmark, we take the period between 2019 and 2020, because of outliers recorded during 2020. The 90% and 95% percentiles of per-capita hourly loads for summer months of this period are 1255.6 and 1317.6 kWh, respectively. In terms of daily peaks of per-capita demand, the corresponding percentiles are 1382.0 and 1444.3 kWh, respectively

**Table 4: Estimated impact <sup>a)</sup> on average hourly loads, by season, decade and RCP scenario**

RCP 4.5			RCP 8.5		
<b>Panel A. Summer</b>					
2020-2030	-0.43	[ -0.73 , -0.12 ]	0.40	[ 0.10 , 0.70 ]	
2030-2040	-0.30	[ -0.71 , -0.10 ]	0.20	[ -0.10 , 0.50 ]	
2040-2050	1.30	[ 0.56 , 1.68 ]	1.48	[ 0.92 , 2.16 ]	
2050-2060	1.82	[ 1.14 , 2.43 ]	3.12	[ 2.45 , 3.82 ]	
2060-2070	2.67	[ 2.05 , 3.18 ]	4.23	[ 3.35 , 4.91 ]	
2070-2080	2.94	[ 2.31 , 3.58 ]	5.42	[ 4.76 , 6.25 ]	
2080-2090	3.24	[ 2.41 , 3.94 ]	6.78	[ 5.42 , 8.02 ]	
2090-2100	4.39	[ 2.56 , 5.06 ]	7.95	[ 6.62 , 9.12 ]	
<b>Panel B. Winter</b>					
2020-2030	-0.02	[ -0.32 , 0.24 ]	-0.04	[ -0.56 , 0.23 ]	
2030-2040	-0.02	[ -0.35 , 0.25 ]	-0.32	[ -0.89 , 0.15 ]	
2040-2050	-0.12	[ -0.57 , 0.16 ]	-1.83	[ -3.01 , -1.13 ]	
2050-2060	-1.06	[ -1.83 , -0.75 ]	-2.45	[ -3.57 , -1.42 ]	
2060-2070	-1.65	[ -2.65 , -1.23 ]	-2.89	[ -3.57 , -1.36 ]	
2070-2080	-1.72	[ -2.82 , -1.34 ]	-2.43	[ -3.53 , -1.25 ]	
2080-2090	-1.73	[ -2.99 , -1.36 ]	-2.40	[ -3.54 , -1.46 ]	
2090-2100	-1.82	[ -3.10 , -1.39 ]	-2.72	[ -3.62 , -1.70 ]	

<sup>a)</sup> Mean and 5%-95% quantiles (in brackets) of bootstrapped differences between hourly loads, projected by RCP data vs baseline forecast based bootstrapped historical temperatures.

**Table 5: Frequencies (%) of hours/days with loads/peak loads exceeding the current\* 90% and 95% percentiles of per-capita electricity demand, by scenario and future periods**

	Exceeding the 90% present percentile			Exceeding the 95% present percentile		
	Baseline	RCP 4.5	RCP 8.5	Baseline	RCP 4.5	RCP 8.5
<b>Panel A. Hourly loads (per-capita)</b>						
2040-2060	32.7	36.2	37.6	25.4	29.0	31.3
2080-2100	61.5	67.5	69.3	53.6	59.8	63.7
<b>Panel B. Daily peaks (per-capita)</b>						
2040-2060	62.8	65.74	67.6	53.2	55.4	57.2
2080-2100	94.0	94.6	97.0	89.0	91.1	94.7

\* As the current period, we use data on summer-month per-capita loads of 2019 and 2020, because of multiple outliers recorded in 2020 due to extremely high temperatures. The 90% and 95% percentiles of per-capita hourly loads for summer months of this period are 1255.6 and 1317.6 kWh, respectively. In terms of daily peaks of per-capita demand, and the corresponding percentiles are 1382.0 and 1444.3 kWh, respectively.

In part, we conclude that in summer months between 2041 and 2060 the occurrence of hours exceeding the present 90th / 95th percentiles will come to 36.2% and 29.0%, respectively under RCP 4.5, and to 37.6% and 31.3%, respectively under RCP 8.5. For the baseline scenario, the corresponding frequencies are 61.5% and 53.6%.

Figure 8 shows the predicted distributions of annual peak load (per-capita), calculated basing on hourly simulations with applied function of annual maximum bootstrap suggested in the MEFM model. As can be seen, density forecasts made with RCP 4.5 and 8.5 summer temperatures shift right—indicating an increment in annual peak load—relative to the baseline of between 1.5% and 5.0%, by the middle of century. Relative to the baseline, the RCP forecasts demonstrate a gradual shift of the probability mass to the right for summer months and to the left for winter months, thus providing evidence that future annual peaks are likely to come from summer rather than from winter seasons.

The impact of rising temperatures in the Israeli location may be amplified under high relative humidity (Heat stress). Figure 8 illustrates this phenomena, by plotting the U-shape dependence of daily peak loads (in log-terms, adjusted for low-frequency and calendar effects), on daily maximum temperatures, while accounting for high/low relative humidity levels (below/above 68%, which is the median level recorded by the Beit-Dagan station). At high temperatures (35 ° C or more), the gap in electricity consumption observed at high and low humidity levels can reach 12% or more, as follows from the difference in log levels on the right tail of the curves.

Therefore, we re-estimate hourly equations while incorporating both temperature and relative humidity retrospective data. Chen (2015) shows some specifications that allow non-linear dependence of electricity demand on both temperature and relative humidity factors. Instead, we proceed with wet-bulb temperatures<sup>10</sup> (herein: wet temperatures) using the IMS formula<sup>11</sup>, while accounting for sea level pressure through the altitude of the IMS station chosen as representative of a given locality.

CORDEX relative humidity predictions have not yet been downscaled by the IMS. The raw data suggest decreasing relative humidity, which could reduce the effects of rising temperatures. However, talks with climatology experts from the IMS reveal doubts in this regard and suggest keeping relative humidity largely at the same level, until the downscaling of CORDEX relative humidity forecasts is completed. Using these assumptions as a proxy and combining seasonally

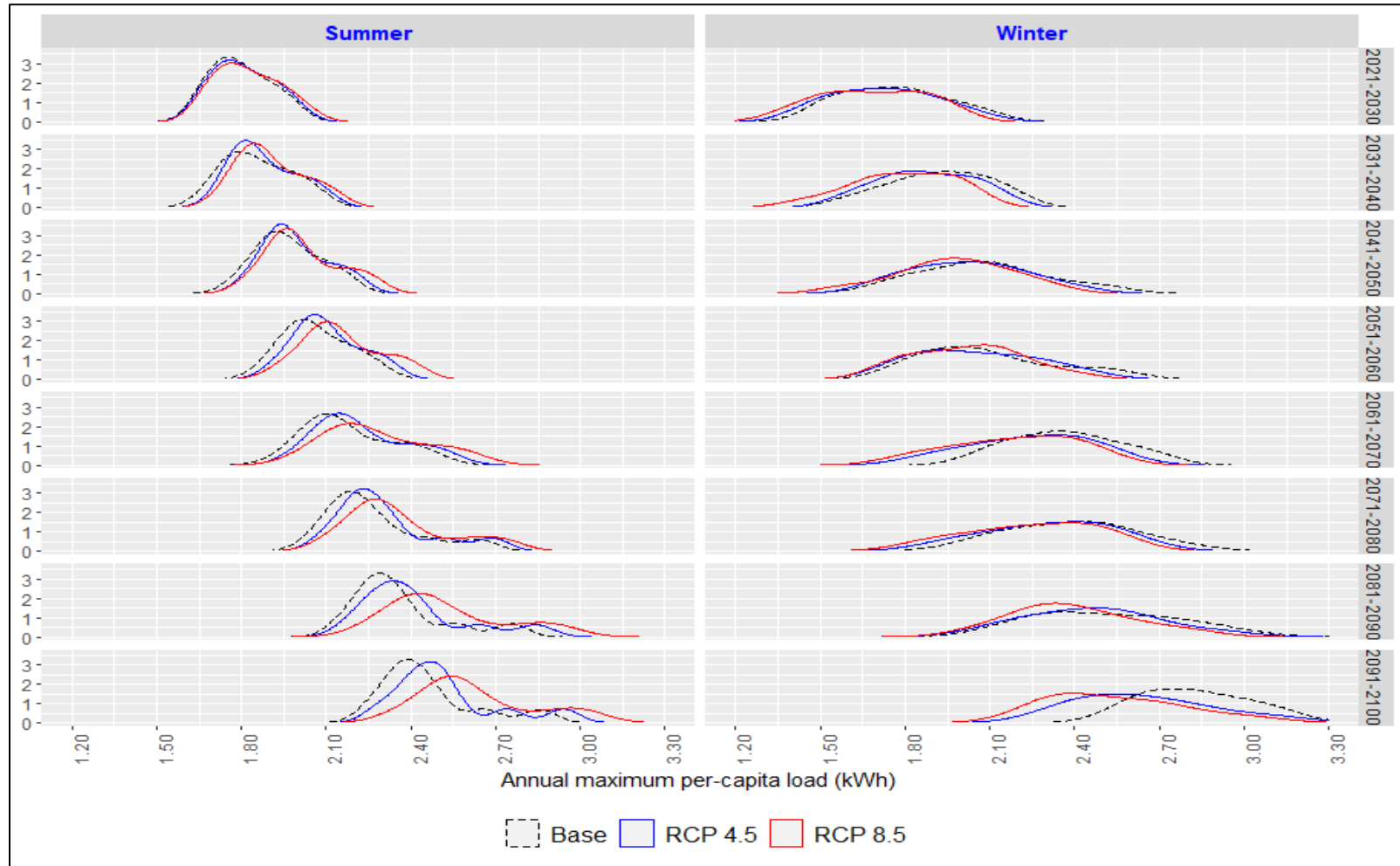
---

<sup>10</sup> For the inter-dependence between wet-bulb temperatures, relative humidity and dry temperatures, we refer to Stull (2011).

<sup>11</sup> See: <https://www.weather.gov/media/epz/wxcalc/wetBulbTdFromRh.pdf>

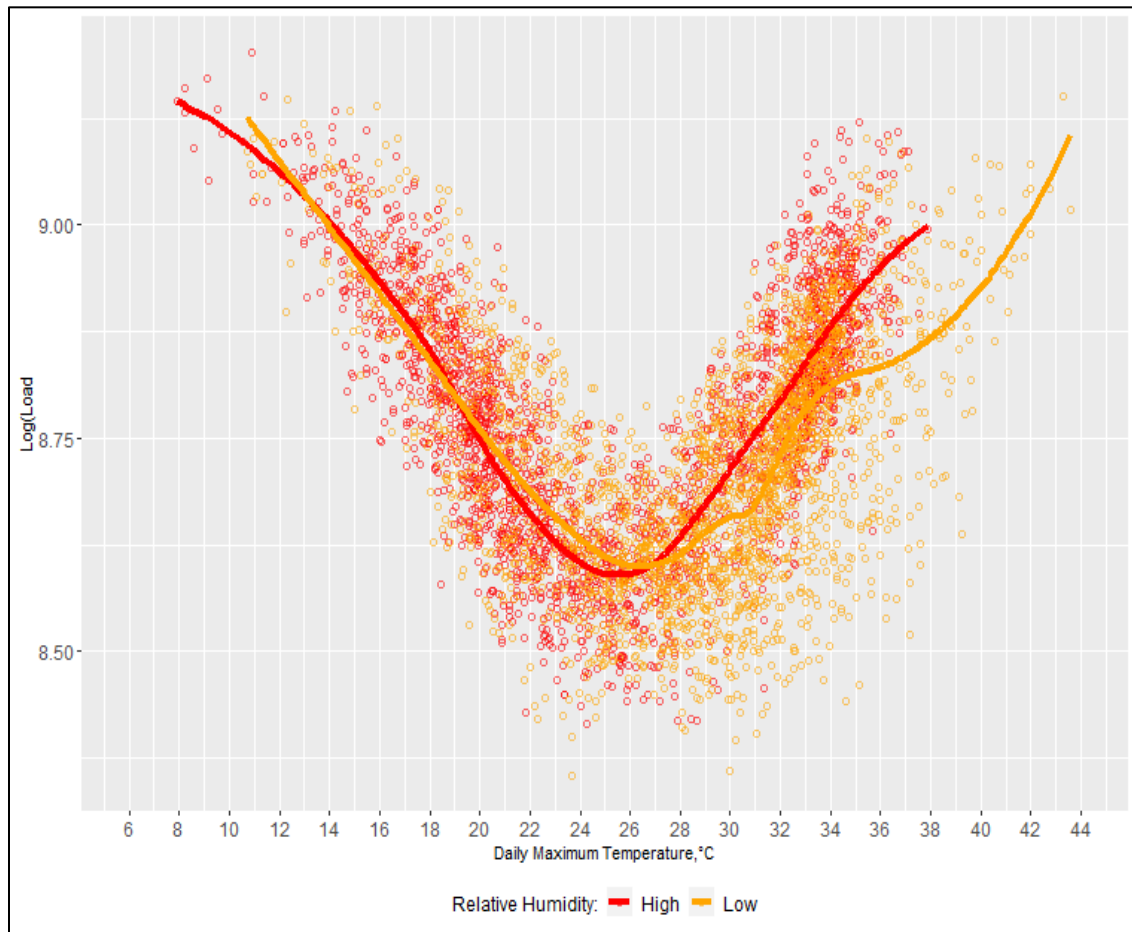
bootstrapped historical levels of relative humidity with the predicted temperatures, we recalculate the predicted impact based on this proxy of wet temperatures. This exercise does not significantly affect the predicted increase in demand compared to previous based on dry temperatures, but expands its confidence interval. More accurate calculations will be possible as soon as downscaled hourly projections of relative humidity by IMS stations become available.

**Figure 8: Distributions<sup>a)</sup> of annual peak per-capita demand (kWh), by season, baseline/RCP scenario and future decades (2021-2100)**



a) Shown are kernel density plots of annual maximum per-capita loads.

**Figure 9: Relative Humidity effect on electricity loads <sup>a)</sup> (2003–19 daily data)**



<sup>a)</sup> In log-terms (Y-axis), adjusted for trend and low-frequency seasonality.

Thus far, our exploration of changes in the intra-daily load curve has focused on the demand side. Planning for meeting increments in future demand relies on the shape of the supply curve as well. Increased reliance on renewable energy sources may impact supply curves, as renewable energy sources may be characterized by less predictable supply and greater variance in maximum output at different times. With renewable energy set to comprise 30% of Israel's total production by the year 2030, impact on maximum capacity for production and intra-daily production curves should be explored.

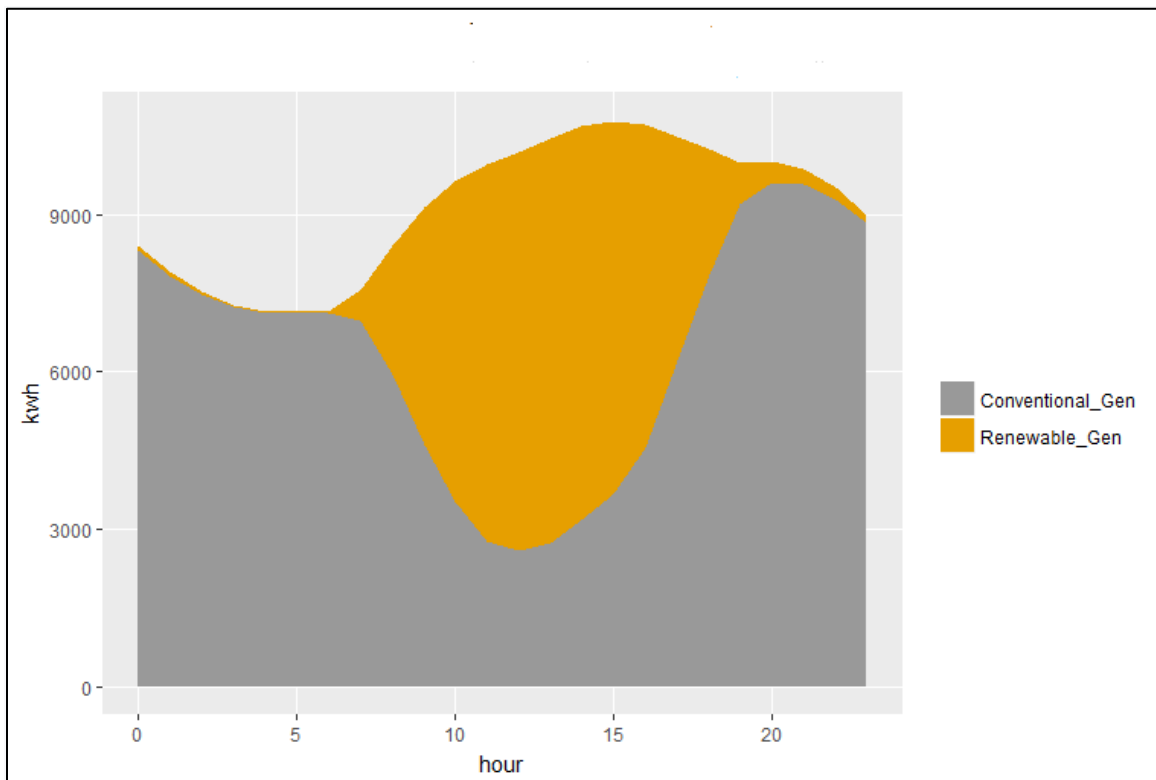
The most widely adopted form of renewable energy in Israel is solar power, made possible by Israel's hot climate and abundance and intensity of sunlit hours. Solar energy production is highest during peak sunlight hours and on sunny days (usually occurring during summer), and drops during cloudier days and during the night. The shape of the load curve using renewable energy is referred to as a "duck curve", referring to the "duck" shape produced by an imbalance in peak production

and peak usage hours, which, in the case of solar energy, causes a surplus during the afternoon on days where peak demand occurs in the evening.

Figure 10 presents a simulation of production on a typical summer's day in 2030, assuming the energy sector has achieved its stated goal of 30% energy production from renewable sources.

Since solar energy production is highest during the afternoon, predicted rises in energy use during peak hours in summer months may be offset by the increased reliance on solar energy, and much of the extra consumption may be met by what would have been a surplus of solar energy. Rising demand during off peak hours could not be offset in a similar manner, as solar energy production during night hours should be nonexistent.

**Figure 10: Conventional and renewable energy production, by hour**  
**Typical summer day in 2030, holding patterns of energy use and total use steady at 2019 levels**



**Note:** Methodology – according to the Israeli Energy Ministry's July 2020 order, energy production from renewable sources in Israel is set to comprise 30% of energy production by 2030. Using 2019 data, we calculate typical hourly distribution of total daily energy production for a summer day, separating renewable and conventional generation. Holding constant intra-daily generation distribution from each energy source as well as total energy usage, we predict typical energy generation for a summer day while assuming 30% of total generation will stem from renewable energy, then redistribute it over the hours of the day. Results are plotted, showing the "duck curve", where peak generation will occur during afternoon hours, bridging part of the surplus demand.

## 5. Conclusions

This study was motivated by the need to quantify the impact of climate change on electricity demand in Israel, regarding further implications on future planning of generation capacity and electricity grid, heavily dependent of expected peak loads. As shown, the impact in Israel may be more severe than in other hot developed countries due to the higher sensitivity of Israeli electricity demand to rising temperatures. Lower sensitivity could be achieved through flexible intra-daily electricity tariffs and transparent timely information for the public.

We document the main increase in daily peak loads during summer months, which are likely to rise more than average daily loads. For winter months, we expect a more moderate gradual decrease of daily peak loads by the end of century. Compared to the present situation, the intensity of summer peaks is likely to rise. Our results also provide evidence that annual peak loads are likely to come from summer months under RCP scenarios.

A large part of the surplus demand expected for summer months can be met with solar energy generation.

## References

Climate change in Israel: past trends and forecast trends in the temperature and precipitation regime "- November 2019, Research Report No. 4000-0804-2019-0000075 – Israeli Meteorological Service, Ministry of Transportation.

Ahmed. T, K.M. Muttaqi and A.P. Agalgaonkar (2012). "Climate change impacts on electricity demand in the State of New South Wales, Australia", *Applied Energy*, 2012; 98: 376–383.

Auffhammer M (2014). "Cooling China: The weather dependence of air conditioner adoption", *Frontiers of Economics in China*, 2014, 9 (1): 70–84.

Auffhammer M, P.Baylis and C.H. Hausman (2017). "Climate change is projected to have severe impacts on the frequency and intensity of peak electricity demand across the United States", *Proc Natl Acad Sci USA*, 114: 1886–1891.

Argov, E. and S. Tsur (2019). "A long-run growth model for Israel" – Bank of Israel, Discussion Paper No. 2019.04.

Bas J. van Ruijven, E. De Cian and I.S. Wing (2019). "Amplification of future energy demand growth due to climate change", *Nature Communications*, 10:2762.

Bobmann, T. and I. Staffel (2015). "The Shape of Future Electricity Demand: Exploring Load Curves in 2050s Germany and Britain", URL: <http://dx.doi.org/10.1016/j.energy.2015.06.082>.

Damm, A. et al. (2017). "Impacts of +2 °C global warming on electricity demand in Europe", *Climate Services*, 2017, 7: 12-30.

Deschenes, O. and Greenstone, M. (2011). "Climate change, mortality, and adaptation: Evidence from annual fluctuations in weather in the US", *American Economic Journal: Applied Economics*, 2011, 3(4): 152–185.

Emodi, N.V. et al. (2018). "The impact of climate change on electricity demand in Australia", *Energy & Environment*, 29 (1): 2018.

Franco, G and A. H. Sanstad (2008). "Climate change and electricity demand in California", *Climatic Change*, 2008, 87(S1):139-151.

Giannakopoulos C. et al. (2016). "Climate change impacts, vulnerability and adaptive capacity of the electrical energy sector in Cyprus", *Regional Environmental Change*, 16, p.p.1891–1904.

Hyndman, R.J. and S. Fan (2015). "Monash Electricity Forecasting Model", URL: <https://robjhyndman.com/papers/MEFMR1.pdf>

- Lia, Y., W.A. Pizerb and L.Wuc (2018). “Climate change and residential electricity consumption in the Yangtze River Delta, China”, *PNAS*, URL: <https://www.pnas.org/content/pnas/116/2/472.full.pdf>
- Neagu, B.C., Gh. Georgescu and M. Gușă (2011). “Load Curves Characteristics of Consumers Supplied from Electricity Repartition and Distribution Public Systems”, ResearchGate, Project: "Voltage Control in Electricity Distribution System".
- Pilli-Sihvola, K, Aatola, P, Ollikainen, M. (2010). “Climate change and electricity consumption—witnessing increasing or decreasing use and costs?”, *Energy Policy 2010*; 38: 2409–2419.
- Stull, R. (2011). “Wet-Bulb Temperature from Relative Humidity and Air Temperature”, *Journal of Applied Meteorology and Climatology*, 2011; 50, 2267-2269.
- Suhoy, T. (2017). “Long-term probabilistic forecast of peak electricity demand (in Hebrew)”, Bank of Israel, Working Paper Series, 2017.12.
- Véliz, K.D., R.K. Kaufmann and C.J. Cleveland (2017). “The effect of climate change on electricity expenditures in Massachusetts”, *Energy Policy 2017*; 106: 1–11.
- Wenz L, A. Levermann and M. Auffhammer (2017). “North–south polarization of European electricity consumption under future warming”, *Proc Natl Acad Sci USA*, 114: E7910– E7918.

## Appendix A. Description of data used

**Table A1: Retrospective data**

	Frequency	Region	Source	From Date	To Date
<b>Electricity Load</b>	Hourly	Israel	Israel Electric Corporation (IEC)	01/01/2002	31/12/2019
		Australia <sup>a)</sup>	Australia Energy Market Operator (AEMO)	01/01/2000 <sup>c)</sup>	31/12/2019
		Texas <sup>b)</sup>	Electric Reliability Council of Texas (ERCOT)	01/01/2002	31/08/2019
<b>Temperature (max)</b>	Daily	Israel	Israel Meteorological Service (IMS)	01/01/2002	31/12/2019
		Australia <sup>a)</sup>	Australian Government Bureau of Meteorology (BOM)	01/01/2000 <sup>c)</sup>	31/12/2019
		Texas <sup>b)</sup>	National Centers for Environmental Information (NOAA)	01/01/2000	31/08/2019
<b>Temperature</b>	Hourly	Israel	IMS	01/01/2002	31/12/2019
<b>Relative Humidity</b>	Hourly	Israel	IMS	01/01/2002	31/12/2019
<b>Population</b>	Monthly	Israel	CBS	01/01/2002	31/12/2019
	Yearly	Australia <sup>a)</sup>	Australia Bureau of Statistics (ABS)	01/01/2003	31/12/2019
		Texas <sup>b)</sup>	Texas State Library (TSL)	01/01/2002	31/08/2019

<sup>a)</sup> New South Wales, Queensland, South Australia, Victoria and Tasmania.

<sup>b)</sup> Eight regions served by ERCOT.

<sup>c)</sup> Tasmania – from 01/01/2003.

**Table A2: CORDEX RCP 4.5/8.5 projections (01/01/2020-31/12/2100)**

Variable	Freq.	Country	Source	Models
Daily max. temperature	Daily	Australia Texas	esgf-data.dkrz.de/ search/esgf-dkrz	HADGEM2-ES, GFDL-ESM2M, EC-EARTH, IPSL-CM5A-ESM2M
Daily max. temperature	Daily	Israel	IMS	NOAA, CCCMA, IPSL, CSIRO, MIROC
Temperature	Hourly			

## Appendix A (continued)

**Table A3: Meteorological stations with downscaled RCP data used for regional deviation calculations, with associated District (Nafa) and meteorological attributed region** <sup>a), b)</sup>

IMS Station	Station Number	District (Nafa)	Meteorological Region
Afula	5811	Emek Yizrael	Jezreel Valley
Akko	280	Haifa and Akko	Zevulun Valley
Be'er Sheva	7841	Be'er Sheva	North Western Negev
Beit Jimal	7151	Jerusalem	Judean foothills - South
Besor Farm	3891	Be'er Sheva	Western Negev
Bet Dagan	2523	Ramla and Petah Tiqwa	Gush Dan
Bet Zayda	8730	Emek Yizrael	Kinarot Valley
Dafna	8263	Galil and Golan	Hula Valley
Dorot	7333	Ashkelon	Judean foothills - South
Eilat	9974	Be'er Sheva	Eilat Gulf Southern Arava
En Hahores	1546	Sharon	Northern Sharon
Galed	1192	Emek Yizrael	Plain of Manasseh
Jerusalem	6771	Jerusalem	Judea Mountains
Kefar Blum	8472	Galil and Golan	Hula Valley
Kefar Yehoshua	5501	Emek Yizrael	Jezreel Valley
Lahav	7416	Be'er Sheva	North Western Negev
Negba	3502	Ashkelon	Judean foothills - South
Qevuzat Yavne	3081	Rehovot	Southern Coast
Sede Boqer	8206	Be'er Sheva	North Western Negev
Sede Eliyyahu	9376	Emek Yizrael	Beit Shean Valley
Sedom	9571	Be'er Sheva	Northern Arava
Tavor	5358	Kinneret	Eastern Lower Galilee
Tel Aviv Coast	2410	Tel Aviv and Hadera	Gush Dan
Yotvata	9772	Be'er Sheva	Eilat Gulf Southern Arava
Zefat	4642	Galil and Golan	Eastern Upper Galilee
Zemah	9111	Kinneret	Kinarot Valley

<sup>a)</sup> Judea and Samaria - no IMS stations with long data exist in the area, temperatures from the Jerusalem station were taken as proxy for the entire area.

<sup>b)</sup> Where data from multiple stations was available for a given region, a simple mean of the temperatures was taken.

## Appendix B. Estimation of dose-response functions for selected group of load zones.

For each area (i.e., Israel, 5 Australian states and 8 load zones of ERCOT (Texas State)) we use retrospective data on daily peak loads and daily maximum temperatures from 2002 to 2019 to fit a bin-regression, as follows:

$$L_{z,d} = \sum_{i=1}^{N_z} \alpha_{i,z} B_i(T_{z,d}) + \sum_{j=0}^6 \beta_{j,z} C_{j,d} + \sum_{k=0}^6 \gamma_{k,z} W_{k,d} + \sum_{l=0}^3 \delta_{l,z} S_{l,d} + \Omega_z + \varepsilon_{z,d} \quad (\text{B.1})$$

where  $L_{z,d}$  are daily peak loads in the  $z$ -th zone;  $T_{z,d}$  are daily maximum temperatures in the  $z$ -th zone binned into  $N_z$  intervals of  $3^\circ\text{C}$  width, as follows:

$$B_i(T_{z,d}) = \begin{cases} 1 & \text{if } T_{z,d} \in \text{bin}_i \\ 0 & \text{otherwise} \end{cases}$$

while the first/last temperature bin is defined separately for each load zone by such a way that at least 2% of observations lie below/above its upper/lower boundary. For this reason the number of bins differs between zones;

$C_{j,d}$  are Chebyshev polynomials<sup>12</sup> of degree  $j = 0, \dots, 6$  specified to capture low-frequency factors of electricity demand (such as GDP growth, changes in technology and sectorial composition, demographical and social factors etc.) and given recursively by:

$$C_{j,d} = 2d \cdot C_{j-1,d} - C_{j-2,d} \text{ for } j \geq 2, \text{ with } C_{0,d} = 1 \text{ and } C_{1,d} = d.$$

$W_{j,d}$  are country/state-specific calendar dummies taking value 1 if day of week is  $j$  and 0 otherwise; for Israel, holidays<sup>13</sup> are encoded as Saturdays<sup>14</sup>, i.e.  $W_7 = 1$ , for other countries as Sundays, i.e.  $W_1 = 1$ ; the omitted (reference) trading-day category for Israel is Sunday, for other countries – Monday;

$S_{l,d}$  are quarterly dummies;

$\alpha_{i,z}$   $\beta_{j,z}$   $\gamma_{k,z}$   $\delta_{l,z}$  are regression coefficients,  $\Omega_z$  are country(state)-specific intercepts;

---

<sup>12</sup> See: Juan Carlos Cuestas, J.C. and L.A. Gil-Alana (2015) " Testing for long memory in the presence of non-linear deterministic trends with Chebyshev polynomials" - *Studies in Nonlinear Dynamics & Econometrics*, 2015, 20(1)

<sup>13</sup> Holidays - national holidays in the various countries, as well as state holidays throughout Australia.

<sup>14</sup> Eves and weekdays during Pesach and Rosh Hashana seasons festival week ("Chol Hamoed") are encoded like Fridays (half-day work), i.e.  $W_6 = 1$ .

$\epsilon_{z,d}$  are stochastic error terms.

To make load-temperature response functions compatible, we adjust peak loads for non-temperature impacts, as follows:

$$L_{z,d}^{adj} = L_{z,d} - (\sum_{j=0}^6 \beta_{j,z} C_{j,d} + \sum_{k=0}^6 \gamma_{k,z} W_{k,d} + \sum_{l=0}^3 \delta_{l,z} S_{l,d}) \quad (\text{B.2})$$

then derive mean residual loads corresponding to the least "comfortable" ( $T_{fix1}$ ) and least "uncomfortable" ( $T_{fix2}$ ) daily maximum temperatures, denoted as  $\overline{L_{z,d}^{adj}(T_{fix1})}$  and  $\overline{L_{z,d}^{adj}(T_{fix2})}$  and normalize, as follows:

$$L_{z,d}^{norm} = \frac{L_{z,d}^{adj} - \overline{L_{z,d}^{adj}(T_{fix1})}}{\overline{L_{z,d}^{adj}(T_{fix2})} - \overline{L_{z,d}^{adj}(T_{fix1})}} \quad (\text{B.3})$$

We refer to Wenz et al. (2017) for methodology of searching the most distant values of  $T_{fix1}$  and  $T_{fix2}$  over a large set of European countries with a large spectrum of temperatures. In our case, we consider cooling aspect as the most relevant for projections and set the upper standardization term on  $T_{fix2} = 36.5 \pm 0.5^\circ\text{C}$ ; the lower standardization term is  $T_{fix1} = 22 \pm 0.5^\circ\text{C}$ . Since normalized residual loads are compatible between countries, we combine these data into discrete temperature intervals of  $1^\circ\text{C}$ , calculate the weighted median for each interval, and connect these nodes with a linear spline (Figure 4).

After compiling fitted load  $L_{z,d}^{fitted}$  based future daily maximum temperature simulations, we are able to calculate load projections compatible with country-specific retrospective data through back-transformation:

$$L_{z,d}^{proj} = L_{z,d}^{fitted} (\overline{L_{z,d}^{adj}(T_{fix2})} - \overline{L_{z,d}^{adj}(T_{fix1})}) + \overline{L_{z,d}^{adj}(T_{fix1})} \quad (\text{B.4})$$

## Appendix C

### Main characteristics of regression (1), by country/state/load zone

	Data span (daily)	Daily Tmax range: 2%÷98%	Number of Temp.bins	R <sup>2</sup> -adj	Explanatory variables			
					Chebyshev polynomials <sup>b)</sup>	Significant trading-day dummies <sup>c)</sup>	Quarterly dummies <sup>d)</sup>	Temperature bins
<b>Panel A. Australia</b>								
New South Wales	01/01/2003-31/12/2019	14.7°C ÷ 35°C	8	0.666	***	Friday, Saturday, Sunday	***	***
Queensland	01/01/2003-31/12/2019	18.8°C ÷ 34.7°C	7	0.843	**	Wednesday, Friday, Saturday, Sunday	**	***
South Australia	01/01/2003-31/12/2019	13.2°C ÷ 37.8°C	9	0.735	**	Friday, Saturday, Sunday	***	***
Tasmania	16/05/2005-31/12/2019	9.7°C ÷ 30.5°C	8	0.753	**	All excl. Monday	***	***
Victoria	01/01/2003-31/12/2019	11.6°C ÷ 37.1°C	10	0.798	*	Friday, Saturday, Sunday	**	***
<b>Total NEM<sup>a)</sup></b>	16/05/2005-31/12/2019	15.4°C ÷ 32.5°C	8	0.765	*	Friday, Saturday, Sunday	**	***
<b>Panel B. Israel</b>	01/01/2002-31/12/2019	14.4°C ÷ 36.9°C	9	0.864	***	Friday, Saturday	***	***
<b>Panel C. Texas</b>								
Coast	01/01/2002-31/08/2019	9.7°C ÷ 36.8°C	11	0.861	***	Saturday, Sunday	***	***
South	01/01/2002-31/08/2019	11.3°C ÷ 36.8°C	10	0.856	***	Friday, Saturday, Sunday	***	***
South Central	01/01/2002-31/08/2019	7.4°C ÷ 38.7°C	12	0.848	***	Friday, Saturday, Sunday	***	***
West	01/01/2002-31/08/2019	3.6°C ÷ 38.6°C	14	0.792	-	Wednesday, Saturday, Sunday	***	***
Far West	01/01/2002-31/08/2019	4.9°C ÷ 39.1°C	13	0.970	***	Saturday, Sunday	***	***
North Central	01/01/2002-31/08/2019	4.9°C ÷ 38.9°C	13	0.841	-	Friday, Saturday, Sunday	***	***
East	01/01/2002-31/08/2019	5.7°C ÷ 37.9°C	12	0.811	*	Friday, Saturday, Sunday	***	***
North	01/01/2002-31/08/2019	2.9°C ÷ 40.4°C	14	0.805	-	Saturday, Sunday	*	***
<b>Total ERCOT<sup>a)</sup></b>	01/01/2002-31/08/2019	8.1°C ÷ 37.7°C	11	0.883	***	Friday, Saturday, Sunday	***	***

a) Dependent daily peak loads and explanatory daily maximum temperatures are calculated as population-weighted averages.

b) \*\*\* and \*\* denote significance of at least 4 of 6 polynomials at the 1% and 5% levels, respectively; \* denotes significance of at least 1 polynomial at the 5% level.

c) For Israel holidays are encoded as Saturdays, eves and Chol Hamoed days (half-working days during Pesach and Rosh-Hashana festival season) are encoded as Fridays, the reference (omitted) category is set on Sunday; for other countries holidays are encoded as Sundays and the reference (omitted) category is Monday. Only trading-day effects significant at the 1% level are shown.

d) \*\*\* denote all 3 seasonal dummies are significant at the 1% level; \*\* denotes at least two seasonal dummies are significant at the 5% level, \* denotes at least one seasonal dummy significant at the 5% level.

## Appendix D. MEFM model used for estimation of intra-daily changes

For estimation of intra-daily changes, we implement Hyndman and Fan (2015)'s forecasting model, which handles low- and high-frequency components of observed loads separately. The low-frequency component  $load^{(Q)}$  is the average level of quarterly electricity demand, which can be decomposed into a stochastic trend, a seasonal component, an exogenous effect depending on macroeconomic and population growth, the quarterly number of cooling/heating days, and a residual. This decomposition allows us to forecast quarterly mean levels using an unobservable component model (Suhoy, 2017) and deal with hourly data in terms of log-deviations from the corresponding quarterly (seasonal) mean.

The high-frequency component, defined as the log-deviation of the hourly electricity load from the corresponding quarterly mean has been handled by 24 nonlinear regressions (one for each hour), as follows:

$$y_{t,h} = \alpha_h + c_h(t) + f_h(T_{1,t}, T_{2,t}) + e_{t,h} \quad h = 0, 1, \dots, 23 \quad (D.1)$$

where

$y_{t,h}$  is the log difference between the hourly load data  $load_t$  at time  $t$  and the quarterly average load  $load^{(Q)}$  by hour;

$\alpha_h$  is the specific "fixed" parameter for the hour, estimated together with the other parameters of (D.1) and dependent as well on the seasonal model (summer/winter);

$c_h(t)$  is the calendar effect of the specific time defined via dummy variables as:

$c_h(t) = \sum_{k=1}^6 \gamma_{h,k} W_{k,t} + \tau_h(t)$ .  $W_k$  represent workdays, holidays (such as Saturdays), and holiday eves (such as Fridays), and the parameters  $\gamma_{h,k}$

are estimated simultaneously with the other parameters in (D.1);

$\tau_h(t)$  is the smooth cyclical function of a 183-day cycle for the summer model (observations from April through September ) and of 182 days for the winter model (observations from October through March, excluding February 29 in leap years);

$f_h(T_{1,t}, T_{2,t})$  reflects an hourly component that depends (in a nonlinear fashion) on temperatures recorded in two of the Israel Meteorological Service's stations—in Beit Dagan and Be'ersheva—including hourly and daily lags and weather differences between the stations, defined as follows:

$$X_t = (T_{1,t} + T_{2,t})/2; \quad D_t = (T_{1,t} - T_{2,t});$$

$$\begin{aligned}
f_h(T_{1,t}, T_{2,t}) = & \sum_{p=0}^6 [f_{p,h}(X_{t-h}) + g_{k,h}(D_{t-h})] + \sum_{j=0}^6 [F_{j,h}(X_{t-48j}) + G_{j,h}(D_{t-48j})] + q_h(X_t^+) \\
& + r_h(X_t^-) + s_h(\bar{X}_t) \tag{D.2}
\end{aligned}$$

where  $X_t^+$  is the maximum of  $X_t$  over 24 hours,  $X_t^-$  is the minimum of  $X_t$  over 24 hours,  $\bar{X}_t$  is the average of  $X_t$  over 24 hours; each one of the functions  $f_{p,h}, g_{j,h}, F_{p,h}, G_{j,h}, q_h, r_h, s_h$  is estimated as a second-order spline.

To derive the impact of rising temperatures, we have to project low- and high-frequency components under the baseline (without RCP assumption) and the RCP scenario, and then compare.

Quarterly forecasts for the baseline scenario were estimated based on long-run forecasts of GDP and population growth and seasonal bootstrap of numbers of cooling / heating days<sup>15</sup>, observed quarterly between 2002 and 2019. Quarterly forecasts for each RCP scenario were calculated based the same macroeconomic projections while the quarterly sums of cooling / heating days were derived from CORDEX-simulated daily maximum temperatures, provided by IMS.

Hourly deviations from seasonal mean loads were forecasted using statistical permutation of actually observed hourly temperatures based seasonal bootstrap algorithm described in Hyndman and Fan (2015). High-frequency components for each RCP scenario were projected by hourly temperature simulations, provided by IMS, by five models. For each scenario – either baseline or RCP - high-frequency components include an additional terms, i.e. a residual component simulated based ACF found in-sample and appropriately bootstrapped using Hyndman and Fan (2015) algorithm.

---

<sup>15</sup> We define a cooling day as a day with a daily maximum temperature above 26 °C, a heating day – with a daily maximum temperature below 14 °C.